Laser Cooling and Trapping

Article *in* Journal of the Optical Society of America B · May 2003

DOI: 10.1364/JOSAB.20.000887 · Source: OAI

2 authors, including:

Peter van der Straten
Utrecht University
129 PUBLICATIONS **4,977** CITATIONS

SEE PROFILE

Laser Cooling and Trapping of Neutral Atoms

Q1 *H. J. Metcalf*●
Q2 *Department of Physics, State University of New York, Stony Brook, N.Y. 11794-3800, USA*●.
Q3 *e-mail:*● *H.J.Metcalf@phys.uu.nl*
Q4

Peter van der Straten
Debye Institute, Department of Atomic and Interface Physics, Utrecht University, 3508 TA Utrecht, The Netherlands. e-mail: P.vanderStraten@phys.uu.nl

Abstract
This article presents a review of some of the principal techniques of laser cooling and trapping that have been developed during the past 20 years. Its approach is primarily experimental, but its quantitative descriptions are consistent in notation with most of the theoretical literature.

Keywords
laser cooling; atom trapping; optical lattice; Bose–Einstein condensation.

1 Introduction

The combination of laser cooling and atom trapping has produced astounding new tools for atomic physicists [1]. These experiments require the exchange of momentum between atoms and an optical field, usually at a nearly resonant frequency. The energy of light $\hbar\omega$ changes the internal energy of the atom, and the angular momentum $\hbar$ changes the orbital angular momentum ℓ of the atom, as described by the well-known selection rule $\Delta\ell = \pm 1$. By contrast, the linear momentum of light $p = \hbar\omega/c = \hbar k$ cannot change the internal atomic degrees of freedom, and therefore must change the momentum of the atoms in the laboratory frame. The force resulting from this momentum exchange between the light field and the atoms can be used in many ways to control atomic motion, and is the subject of this article.

1.1 Temperature and Entropy

The idea of ''temperature'' in laser cooling requires some careful discussion and disclaimers. In thermodynamics, temperature is carefully defined as a parameter of the state of a closed system in thermal equilibrium with its surroundings. This, of course, requires that there be thermal contact, that is, heat exchange, with the environment. In laser cooling, this is clearly not the case because a sample of atoms is always absorbing and scattering light. Furthermore, there is essentially no heat exchange (the light cannot be considered as heat even though it is indeed a form of energy). Thus, the system may very well be in a steady state situation, but certainly not in thermal equilibrium, so the assignment of a thermodynamic ''temperature'' is completely inappropriate.

Nevertheless, it is convenient to use the label of temperature to describe an atomic sample whose average kinetic energy $\langle E_k \rangle$ has been reduced by the laser light, and this is written simply as $k_B T/2 = \langle E_k \rangle$, where k_B is the Boltzmann's constant (for the case of one dimension, 1-D). It must be remembered that this temperature assignment is absolutely inadequate for atomic samples that do not have a Maxwell–Boltzmann velocity distribution, whether or not they are in thermal contact with the environment; there are infinitely many velocity distributions that have the same value of $\langle E_k \rangle$ but are so different from one another that characterizing them by the same ''temperature'' is a severe error. (In the special case where there is a true damping force, $F \propto -v$, and where the diffusion in momentum space is a constant independent of momentum, solutions of the Fokker–Planck equation can be found analytically and can lead to a Maxwell–Boltzmann distribution that does indeed have a temperature.)

Since laser cooling decreases the temperature of a sample of atoms, there is less disorder and therefore less entropy. This seems to conflict with the second law of thermodynamics, which requires the entropy of a closed system to always increase with time. The explanation lies in the consideration of the fact that in laser cooling, the atoms do not form a closed system. Instead, there is always a flow of laser light with low entropy into the system and fluorescence with high entropy out of it. The decrease of entropy of the atoms is accompanied by a much larger increase in entropy of the light field. Entropy considerations for a laser beam are far from trivial, but recently it has been shown that the entropy lost by the atoms

is many orders of magnitude smaller than the entropy gained by the light field.

1.2 Phase Space Density

The phase space density $\rho(\vec{r}, \vec{p}, t)$ is defined as the probability that a single particle is in a region $d\vec{r}$ around $\vec{r}$ and has momentum $d\vec{p}$ around $\vec{p}$ at time t. In classical mechanics, $\rho(\vec{r}, \vec{p}, t)$ is just the sum of the $\rho(\vec{r}, \vec{p}, t)$ values of each of the N particles in the system divided by N. Since the phase space density is a probability, it is always positive and can be normalized over the six-dimensional volume spanned by position $\vec{r}$ and momentum $\vec{p}$. For a gas of cold atoms, it is convenient to choose the elementary volume for $\rho(\vec{r}, \vec{p}, t)$ to be $\hbar^3$, so it becomes the dimensionless quantity

$$\rho_\phi = n\lambda_{\mathrm{deB}}^3, \tag{1}$$

where λ_{deB} is the deBroglie wavelength of the atoms in the sample and n is their spatial density.

The Liouville theorem requires that ρ_ϕ cannot be increased by using conservative forces. For instance, in light optics one can focus a parallel beam of light with a lens to a small spot. However, that simply produces a high density of light rays in the focus in exchange for the momentum part of ρ_ϕ because the beam entering the lens is parallel but the light rays are divergent at the focus.

For classical particles, the same principle applies. By increasing the strength of the trapping potential of particles in a trap, one can increase the density of the atoms in the trap but at the same time, the compression of the sample results in a temperature increase, leaving the phase space density unchanged.

In order to increase the phase space density of an atomic sample, it is necessary to use a force that is not conservative, such as a velocity-dependent force. In laser cooling, the force on the atoms can be a damping force, that is, always directed opposite to the atomic velocity, so that the momentum part of ρ_ϕ increases. This process arises from the irreversible nature of spontaneous emission.

2 Optical Forces on Neutral Atoms

The usual form of electromagnetic forces is given by $\vec{F} = q(\vec{\mathcal{E}} + \vec{v} \times \vec{B})$, but for neutral atoms, $q = 0$. The next order of force is the dipole term, but this also vanishes because neutral atoms have no inherent dipole moment. However, a dipole moment can be induced by a field, and this is most efficient if the field is alternating near the atomic resonance frequency. Since these frequencies are typically in the optical range, dipole moments are efficiently induced by shining nearly resonant light on the atoms.

If the light is absorbed, the atom makes a transition to the excited state, and the subsequent return to the ground state can be either by spontaneous or by stimulated emission. The nature of the optical force that arises from these two different processes is quite different and will be described separately.

The spontaneous emission case is different from the familiar quantum-mechanical calculations using state vectors to describe the system. Spontaneous emission causes the state of the system to evolve from a pure state into a mixed state and so the density matrix is needed to describe it. Spontaneous emission is an essential ingredient for the dissipative nature of the optical forces.

2.1 Radiative Optical Forces

In the simplest case–the absorption of well-directed light from a laser beam–the momentum exchange between the light field and the atoms results in a force

$$\vec{F} = \frac{\mathrm{d}\vec{p}}{\mathrm{d}t} = \hbar\vec{k}\gamma_p, \qquad (2)$$

where γ_p is the excitation rate of the atoms. The absorption leaves the atoms in their excited state, and if the light intensity is low enough that they are much more likely to return to the ground state by spontaneous emission than by stimulated emission, the resulting fluorescent light carries off momentum $\hbar k$ in a random direction. The momentum exchange from the fluorescence averages zero, so the net total force is given by Eq. (2).

The excitation rate γ_p depends on the laser detuning from atomic resonance $\delta \equiv \omega_\mathrm{l} - \omega_\mathrm{a}$, where ω_l is the laser frequency and ω_a is the atomic resonance frequency. This detuning is measured in the atomic rest frame, and it is necessary that the Doppler-shifted laser frequency in the rest frame of the moving atoms be used to calculate γ_p. In Sect. 2.3.3, we find that γ_p for a two-level atom is given by the Lorentzian

$$\gamma_p = \frac{s_0\gamma/2}{1 + s_0 + [2(\delta + \omega_\mathrm{D})/\gamma]^2}, \qquad (3)$$

where $\gamma \equiv 1/\tau$ is an angular frequency corresponding to the natural decay rate of the excited state. Here, $s_0 = I/I_\mathrm{s}$ is the ratio of the light intensity I to the saturation intensity $I_\mathrm{s} \equiv \pi hc/3\lambda^3\tau$, which is a few mW cm^{-2} for typical atomic transitions. The Doppler shift seen by the moving atoms is $\omega_\mathrm{D} = -\vec{k}\cdot\vec{v}$ (note that $\vec{k}$ opposite to $\vec{v}$ produces a positive Doppler shift for the atoms). The force is thus velocity-dependent and the experimenters' task is to exploit this dependence to the desired goal, for example, optical friction for laser cooling.

The maximum attainable deceleration is obtained for high intensities of light. High-intensity light can produce faster absorption, but it also causes equally fast stimulated emission; the combination produces neither deceleration nor cooling. The momentum transfer to the atoms by stimulated emission is in the opposite direction to what it was in absorption, resulting in a net transfer of zero momentum●. Q5 At high intensity, Eq. (3) shows saturation of γ_p at $\gamma/2$, and since the force is given by Eq. (2), the deceleration saturates at a value $\vec{a}_\mathrm{max} = \hbar\vec{k}\gamma/2M$.

2.2 Dipole Optical Forces

While detuning ●$|\delta| \gg \gamma$, spontaneous emission may be much less frequent than Q6 stimulated emission, unlike the case of the dissipative radiative force that is necessary for laser cooling, given by Eqs. (2) and (3). In this case, absorption is most often followed by stimulated emission, and seems to produce zero momentum transfer because the stimulated light has the same momentum as the exciting light. However, if the optical field has beams with at least two different $\vec{k}$-vectors present, such as in counterpropagating beams, absorption from one beam followed by stimulated emission into the other indeed produces a nonzero momentum exchange. The result is called the dipole force, and is reversible and hence conservative, so it cannot be used for laser cooling.

The dipole force is more easily calculated from an energy picture than from a momentum picture. The force then derives

from the gradient of the potential of an atom in an inhomogeneous light field, which is appropriate because the force is conservative. The potential arises from the shift of the atomic energy levels in the light field, appropriately called the "light shift", and is found by direct solution of the Schrödinger equation for a two-level atom in a monochromatic plane wave. After making both the dipole and rotating wave approximations, the Hamiltonian can be written as

$$\mathcal{H} = \frac{\hbar}{2}\begin{bmatrix} -2\delta & \Omega \\ \Omega^* & 0 \end{bmatrix} \tag{4}$$

where the Rabi frequency is $|\Omega| = \gamma\sqrt{s_0/2}$ for a single traveling laser beam. Solution of Eq. (4) for its eigenvalues provides the dressed state energies that are light-shifted by

$$\omega_{\rm ls} = \frac{\left[\sqrt{|\Omega|^2 + \delta^2} - \delta\right]}{2}. \tag{5}$$

For sufficiently large detuning $|\delta| \gg |\Omega|$, approximation of Eq. (5) leads to $\omega_{\rm ls} \approx |\Omega|^2/4\delta = \gamma^2 s_0/8\delta$.

In a standing wave in 1-D with $|\delta| \gg |\Omega|$, the light shift $\omega_{\rm ls}$ varies sinusoidally from node to antinode. When δ is sufficiently large, the spontaneous emission rate may be negligible compared with that of stimulated emission, so that $\hbar\omega_{\rm ls}$ may be treated as a potential U. The resulting dipole force is

$$\vec{F} = -\vec{\nabla}U = -\frac{\hbar\gamma^2}{8\delta I_{\rm s}}\vec{\nabla}I, \tag{6}$$

where I is the total intensity distribution of the standing-wave light field of period $\lambda/2$. For such a standing wave, the optical electric field (and the Rabi frequency) at the antinodes is double that of each traveling wave that composes it, and so the total intensity $I_{\rm max}$ at the antinodes is four times that of the single traveling wave.

2.3 Density Matrix Description of Optical Forces

2.3.1 Introduction

Use of the density matrix ρ for pure states provides an alternative description to the more familiar one that uses wave functions and operators but adds nothing new. Its equation of motion is $i\hbar(\mathrm{d}\rho/\mathrm{d}t) = [\mathcal{H}, \rho]$, and can be derived directly from the Schrödinger equation. Moreover, it is a straightforward exercise to show that the expectation value of any operator $\mathcal{A}$ that represents an observable is $\langle\mathcal{A}\rangle = \mathrm{tr}\,(\rho\mathcal{A})$.

Application of the Ehrenfest theorem gives the expectation value of the force as $\langle F\rangle = -\mathrm{tr}\,(\rho\nabla\mathcal{H})$. Beginning with the two-level atom Hamiltonian of Eq. (4), we find the force in 1-D to be

$$\langle F\rangle = \hbar\left(\frac{\partial\Omega}{\partial z}\rho_{eg}^* + \frac{\partial\Omega^*}{\partial z}\rho_{eg}\right). \tag{7}$$

Thus, $\langle F\rangle$ depends only on the off-diagonal elements $\rho_{eg} = \rho_{ge}^*$, terms that are called *the optical coherences*.

2.3.2 Open Systems and the Dissipative Force

The real value of the density matrix formalism for atom-light interactions is its ability to deal with open systems. By not including the fluorescent light that is lost from an atom-laser system undergoing cooling, a serious omission is being made in the discussion above. That is, the closed system of atom plus laser light that can be described by Schrödinger wave functions and is thus in a pure state, undergoes evolution to a "mixed" state by virtue of the spontaneous emission. This omission can be rectified by simple ad hoc additions

to the equation of motion, and the result is called the optical Bloch equations (OBE). These are written explicitly as

$$\begin{aligned}
\frac{\mathrm{d}\rho_{gg}}{\mathrm{d}t} &= +\gamma\rho_{ee} + \frac{i}{2}(\Omega^*\tilde{\rho}_{eg} - \Omega\tilde{\rho}_{ge}) \\
\frac{\mathrm{d}\rho_{ee}}{\mathrm{d}t} &= -\gamma\rho_{ee} + \frac{i}{2}(\Omega\tilde{\rho}_{ge} - \Omega^*\tilde{\rho}_{eg}) \\
\frac{\mathrm{d}\tilde{\rho}_{ge}}{\mathrm{d}t} &= -\left(\frac{\gamma}{2} + i\delta\right)\tilde{\rho}_{ge} + \frac{i}{2}\Omega^*(\rho_{ee} - \rho_{gg}) \\
\frac{\mathrm{d}\tilde{\rho}_{eg}}{\mathrm{d}t} &= -\left(\frac{\gamma}{2} - i\delta\right)\tilde{\rho}_{eg} + \frac{i}{2}\Omega(\rho_{gg} - \rho_{ee}),
\end{aligned} \tag{8}$$

where $\tilde{\rho}_{eg} \equiv \rho_{eg}\mathrm{e}^{-i\delta t}$ for the coherences.

In these equations, the terms proportional to the spontaneous decay rate γ have been put in "by hand", that is, they have been introduced into the OBEs to account for the effects of spontaneous emission. The spontaneous emission is irreversible and accounts for the dissipation of the cooling process. For the ground state, the decay of the excited state leads to an increase of its population ρ_{gg} proportional to $\gamma\rho_{ee}$, whereas for the excited state, it leads to a decrease of ρ_{ee}, also proportional to $\gamma\rho_{ee}$. These equations have to be solved in order to evaluate the optical force on the atoms.

2.3.3 Solution of the OBEs in Steady State

In most cases, the laser light is applied for a period long compared to the typical evolution times of atom-light interaction, that is, the lifetime of the excited state $\tau = 1/\gamma$. Thus, only the steady state solution of the OBEs have to be considered, and these are found by setting the time derivatives in Eq. (8) to zero. Then the probability ρ_{ee} to be in the excited state is found to be

$$\rho_{ee} = \frac{\gamma_p}{\gamma} = \frac{s_0/2}{1 + s_0 + (2\delta/\gamma)^2} = \frac{s/2}{1+s}, \tag{9}$$

where $s \equiv s_0/[1 + (2\delta/\gamma)^2]$ is the off-resonance saturation parameter. The excited-state population ρ_{ee} increases linearly with the saturation parameter s for small values of s, but for s of the order of unity, the probability starts to saturate to a value of 1/2. The detuning dependence of γ_p (see Eq. 3) showing this saturation for various values of s_0 is depicted in Fig. 1.

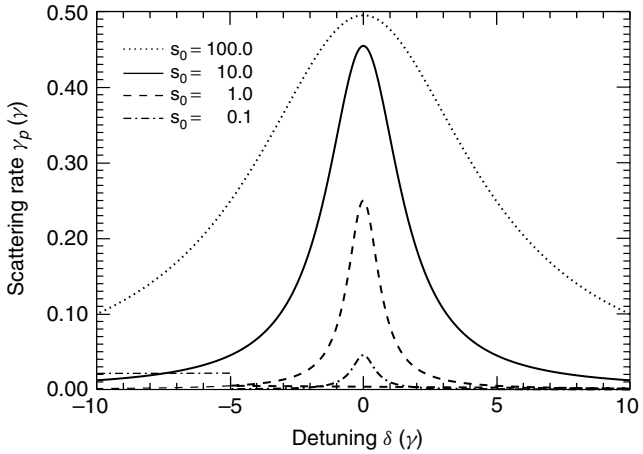

Fig. 1 Excitation rate γ_p as a function of the detuning δ for several values of the saturation parameter s_0. Note that for $s_0 > 1$, the line profiles start to broaden substantially from power broadening

2.3.4 Radiative and Dipole Forces

Some insight into these forces emerges by expressing the gradient of the Rabi frequency of Eq. (7) in terms of a real and imaginary part so that $(\partial\Omega/\partial z) = (q_r + iq_i)\Omega$. Then Eq. (7) becomes

$$F = \hbar q_r(\Omega\rho_{eg}^* + \Omega^*\rho_{eg}) + i\hbar q_i(\Omega\rho_{eg}^* - \Omega^*\rho_{eg}) \quad (10)$$

Thus, the first term of the force is related to the dispersive part of the atom-light interaction, whereas the second term is related to the absorptive part of the atom-light interaction.

To appreciate the utility of the separation of $\nabla\Omega$ into real and imaginary parts, consider the interaction of atoms with a traveling plane wave $\mathcal{E}(z) = \mathcal{E}_0(e^{i(kz-\omega t)} + \text{c.c.})/2$. In this case, $q_r = 0$ and $q_i = k$, and so the force is caused only by absorption. The force is given by $F_{sp} = \hbar k\gamma\rho_{ee}$ and is the radiative force of Eqs. (2) and (3).

For the case of counterpropagating plane waves, there is a standing wave whose electric field is $\mathcal{E}(z) = \mathcal{E}_0\cos(kz)(e^{-i\omega t} + \text{c.c.})$. Thus, $q_r = -k\tan(kz)$ and $q_i = 0$, so there is only the dispersive part of the force, given by

$$F_{dip} = \frac{2\hbar k\delta s_0 \sin 2kz}{1 + 4s_0\cos^2 kz + (2\delta/\gamma)^2}. \quad (11)$$

This replaces Eq. (6) for the dipole force and removes the restriction $|\delta| \gg |\Omega|$, thereby including saturation effects. Even though the average of this force over a wavelength vanishes, it can be used to trap atoms in a region smaller than the wavelength of the light.

2.3.5 Force on Moving Atoms

In order to show how these forces can be used to cool atoms, one has to consider the force on moving atoms. For the case of atomic velocities that are small compared with γ/k, the motion can be treated as a small perturbation in the atomic evolution that occurs on the time scale $1/\gamma$. Then the first-order result is given by

$$\frac{d\Omega}{dt} = \frac{\partial\Omega}{\partial t} + v\frac{\partial\Omega}{\partial z} = \frac{\partial\Omega}{\partial t} + v(q_r + iq_i)\Omega. \quad (12)$$

For the case of atoms moving in a standing wave, this results in the same damping force as Eq. (13) below.

3 Laser Cooling

3.1 Slowing Atomic Beams

Among the earliest laser cooling experiments was the deceleration of atoms in a beam [2]. The authors exploited the Doppler shift to make the momentum exchange (hence the force) velocity dependent. It worked by directing a laser beam opposite an atomic beam so that the atoms could absorb light, and hence momentum $\hbar k$, very many times along their paths through the apparatus as shown in Fig. 2 [2, 3]. Of course, excited-state atoms cannot absorb light efficiently from the laser that excited them, so between absorptions they must return to the ground state by spontaneous decay, accompanied by the emission of fluorescent light. The spatial symmetry of the emitted fluorescence results in an average of zero net momentum transfer from many such fluorescence events. Thus, the net force on the atoms is in the direction of the laser beam, and the maximum deceleration is limited by the spontaneous emission rate γ.

Since the maximum deceleration $\vec{a}_{max} = \hbar\vec{k}\gamma/2M$ is fixed by atomic parameters, it is straightforward to calculate the minimum

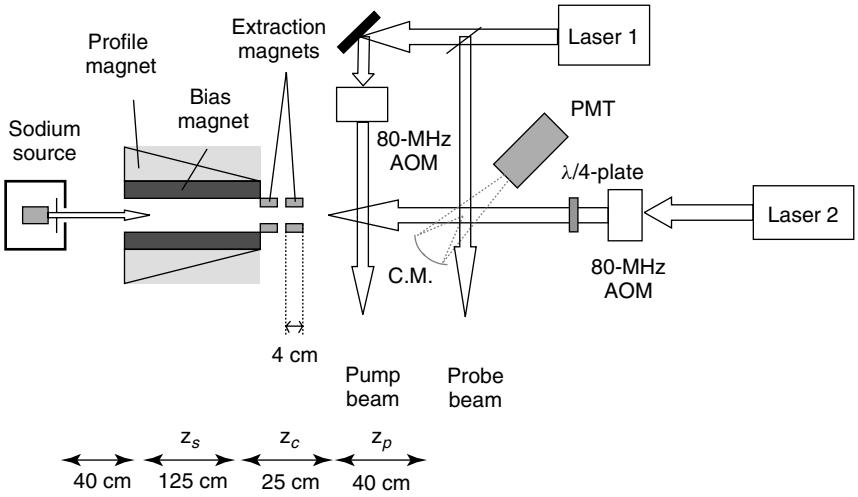

Fig. 2 Schematic diagram of apparatus for beam slowing. The tapered magnetic field is produced by layers of varying length on the solenoid

stopping length $L_{\min}$ and time $t_{\min}$ for the rms velocity of atoms $\bar{v} = 2\sqrt{k_B T/M}$ at the source temperature. The result is $L_{\min} = \bar{v}^2/2a_{\max}$ and $t_{\min} = \bar{v}/a_{\max}$. In Table 1 are some of the parameters for slowing a few atomic species of interest from the peak of the thermal velocity distribution.

Maximizing the scattering rate γ_p requires $\delta = -\omega_D$ in Eq. (3). If δ is chosen for a particular atomic velocity in the beam, then as the atoms slow down, their changing Doppler shift will take them out of resonance. They will eventually cease deceleration after their Doppler shift has been decreased by a few times the power-broadened width $\gamma' = \gamma\sqrt{1+s_0}$, corresponding to Δv of a few times $v_c = \gamma'/k$. Although this Δv of a few m s^{-1} is considerably larger than the typical atomic recoil velocity $v_r = \hbar k/M$ of a few cm s^{-1}, it is still only a small fraction of the average thermal velocity $\bar{v}$ of the atoms, such that significant further cooling or deceleration cannot be accomplished.

Tab. 1 Parameters of interest for slowing various atoms. The stopping length $L_{\min}$ and time $t_{\min}$ are minimum values. The oven temperature T_{oven} that determines the peak velocity is chosen to give a vapor pressure of 1 Torr. Special cases are H at 1000 K for dissociation of H_2 into atoms, and He in the metastable triplet state, for which two rows are shown: one for a 4-K source and another for the typical discharge temperature

Atom	T_{oven} *(K)*	$\bar{v}$ *(m s^{-1})*	L_{min} *(m)*	t_{min} *(ms)*
H	1000	5000	0.012	0.005
He*	4	158	0.03	0.34
He*	650	2013	4.4	4.4
Li	1017	2051	1.15	1.12
Na	712	876	0.42	0.96
K	617	626	0.77	2.45
Rb	568	402	0.75	3.72
Cs	544	319	0.93	5.82

In order to achieve deceleration that changes the atomic speeds by hundreds of m s^{-1}, it is necessary to maintain $(\delta + \omega_D) \ll \gamma$ by compensating such large changes of the Doppler shift. This can be

done by changing ω_D through the angular dependence of $\vec{k} \cdot \vec{v}$, or changing δ either via ω_l or ω_a. The two most common methods for maintaining this resonance are sweeping the laser frequency ω_l along with the changing ω_D of the decelerating atoms [4–6], or by spatially varying the atomic resonance frequency with an inhomogeneous d.c magnetic field to keep the decelerating atoms in resonance with the fixed frequency laser [2, 3, 7].

The use of a spatially varying magnetic field to tune the atomic levels along the beam path was the first method to succeed in slowing atoms [2, 3]. It works as long as the Zeeman shifts of the ground and excited states are different so that the resonant frequency is shifted. The field can be tailored to provide the appropriate Doppler shift along the moving atom's path. A solenoid that can produce such a spatially varying field has layers of decreasing lengths. The technical problem of extracting the beam of slow atoms from the end of the solenoid can be simplified by reversing the field gradient and choosing a transition whose frequency decreases with increasing field [9].

For alkali atoms such as sodium, a time-of-flight (TOF) method can be used to measure the velocity distribution of atoms in the beam [8]. It employs two additional beams labeled pump and probe from Laser 1 as shown in Fig. 2. Because these beams cross the atomic beam at 90°, $\omega_D = -\vec{k} \cdot \vec{v} = 0$, and they excite atoms at all velocities. The pump beam is tuned to excite and empty a selected ground hyperfine state (hfs), and it transfers more than 98% of the population as the atoms pass through its 0.5 mm width. To measure the velocity distribution of atoms in the selected hfs, this pump laser beam is interrupted for a period of $\Delta t = 10 - 50\,\mu s$ with an acoustic optical modulator (AOM). A pulse of atoms in the selected hfs passes the pump region and travels to the probe beam. The time dependence of the fluorescence induced by the probe laser, tuned to excite the selected hfs, gives the time of arrival, and this signal is readily converted to a velocity distribution. Figure 3 shows the measured velocity distribution of the atoms slowed by Laser 2.

3.2 Optical Molasses

3.2.1 Doppler Cooling

A different kind of radiative force arises in low intensity, counterpropagating light beams that form a weak standing wave. It is straightforward to calculate the radiative force on atoms moving in such a standing wave using Eq. (3). In the low intensity case where stimulated emission is not important, the forces from the two light beams are simply added to give $\vec{F}_{OM} =$

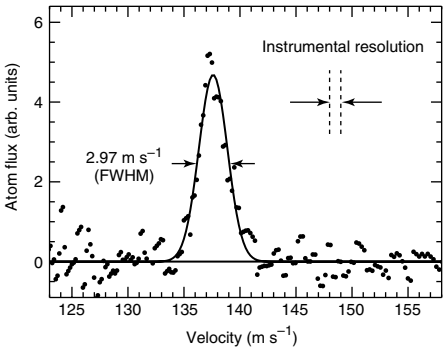

Fig. 3 The velocity distribution measured with the TOF method. The experimental width of approximately $\frac{1}{6}(\gamma/k)$ is shown by the dashed vertical lines between the arrows. The Gaussian fit through the data yields an FWHM● of 2.97 m s^{-1} (figure taken from Molenaar, P. A., vander Straten, P., Heideman, H. G. M., Metcalf, H. (**1997**), *Phys. Rev. A* **55**, 605–614) Q7

$\vec{F}_+ + \vec{F}_-$, where $\vec{F}_\pm$ are found from Eqs. (2) and (3). Then the sum of the two forces is

$$\vec{F}_{\mathrm{OM}} \cong \frac{8\hbar k^2 \delta s_0 \vec{v}}{\gamma(1 + s_0 + (2\delta/\gamma)^2)^2} \equiv -\beta\vec{v}, \tag{13}$$

where terms of order $(kv/\gamma)^4$ and higher have been neglected. The force is proportional to velocity for small enough velocities, resulting in viscous damping for $\delta < 0$ [10, 11] that gives this technique the name "optical molasses" (OM).

These forces are plotted in Fig. 4. For $\delta < 0$, this force opposes the velocity and therefore viscously damps the atomic motion. The force $\vec{F}_{\mathrm{OM}}$ has maxima near $v \approx \pm\gamma\sqrt{s_0} + 1/2k$ and decreases rapidly for larger velocities.

3.2.2 Doppler Cooling Limit

If there were no other influence on the atomic motion, all atoms would quickly decelerate to $v = 0$ and the sample would reach $T = 0$, a clearly unphysical result. In laser cooling and related aspects of optical control of atomic motion, the forces arise because of the exchange of momentum between the atoms and the laser field. These necessarily discrete steps of size $\hbar k$ constitute a heating mechanism that must be considered.

Since the atomic momentum changes by $\hbar k$, their kinetic energy changes on an average by at least the recoil energy $E_{\mathrm{r}} = \hbar^2 k^2/2M = \hbar\omega_{\mathrm{r}}$. This means that the average frequency of each absorption is at least $\omega_{\mathrm{abs}} = \omega_{\mathrm{a}} + \omega_{\mathrm{r}}$. Similarly, the energy $\hbar\omega_{\mathrm{a}}$ available from each spontaneous decay must be shared between the outgoing light and the kinetic energy of the atom recoiling with momentum $\hbar k$. Thus, the average frequency of each emission is $\omega_{\mathrm{emit}} = \omega_{\mathrm{a}} - \omega_{\mathrm{r}}$. Therefore, the light field loses an average energy of $\hbar(\omega_{\mathrm{abs}} - \omega_{\mathrm{emit}}) = 2\hbar\omega_{\mathrm{r}}$ for each scattering event. This loss occurs at a rate of $2\gamma_p$ (two beams), and the energy is converted to atomic kinetic energy because the atoms

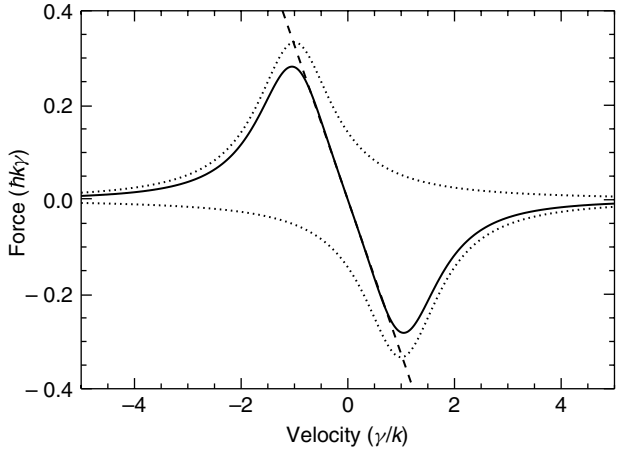

Fig. 4 Velocity dependence of the optical damping forces for 1-D optical molasses. The two dotted traces show the force from each beam, and the solid curve is their sum. The straight line shows how this force mimics a pure damping force over a restricted velocity range. These are calculated for $s_0 = 2$ and $\delta = -\gamma$, so there is some power broadening evident

recoil from each event. The atomic sample is thereby heated because these recoils are in random directions.

The competition between this heating and the damping force of Eq. (13) results in a nonzero kinetic energy in steady state, where the rates of heating and cooling are equal. Equating the cooling rate, $\vec{F}_{\mathrm{OM}} \cdot \vec{v}$, to the heating rate, $4\hbar\omega_{\mathrm{r}}\gamma_p$, we find the steady state kinetic energy to be $(\hbar\gamma/8)(2|\delta|/\gamma + \gamma/2|\delta|)$. This result is dependent on $|\delta|$, and has a minimum at $2|\delta|/\gamma = 1$, whence $\delta = -\gamma/2$. The temperature found from the kinetic energy is then $T_{\mathrm{D}} = \hbar\gamma/2k_{\mathrm{B}}$, where T_{D} is called the Doppler temperature or the Doppler cooling limit. For ordinary atomic transitions, T_{D} is typically below 1 mK.

Another instructive way to determine T_{D} is to note that the average momentum transfer of many spontaneous emissions is zero, but the rms scatter of these about zero is finite. One can imagine these decays as causing a random walk in momentum space, similar to Brownian motion in real space, with step size $\hbar k$ and step frequency $2\gamma_p$, where the factor of 2 arises because of the two beams. The random walk results in an evolution of the momentum distribution as described by the Fokker–Planck equation, and can be used for a more formal treatment of laser cooling. It results in diffusion in momentum space with diffusion coefficient $D_0 \equiv 2(\Delta p)^2/\Delta t = 4\gamma_p(\hbar k)^2$. Then the steady state temperature is given by $k_{\mathrm{B}}T = D_0/\beta$. This turns out to be $\hbar\gamma/2$ as above for the case $s_0 \ll 1$ when $\delta = -\gamma/2$. This remarkable result predicts that the final temperature of atoms in OM is independent of the optical wavelength, atomic mass, and laser intensity (as long as it is not too large).

3.2.3 Atomic Beam Collimation – One-dimensional Optical Molasses – Beam Brightening

When an atomic beam crosses a 1-D OM as shown in Fig. 5, the transverse motion of the atoms is quickly damped while the longitudinal component is essentially unchanged. This transverse cooling of

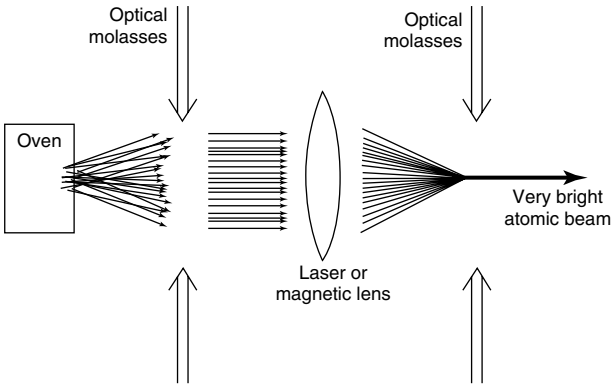

Fig. 5 Scheme for optical brightening of an atomic beam. First, the transverse velocity components of the atoms are damped out by an optical molasses, then the atoms are focused to a spot, and finally the atoms are recollimated in a second optical molasses (figure taken from Sheehy, B., Shang, S. Q., vander Straten, P., Metcalf, H. (**1990**), *Chem. Phys.* **145**, 317–325)

an atomic beam is an example of a method that can actually increase its brightness (atoms/s-sr-cm^2) because such active collimation uses dissipative forces to compress the phase space volume occupied by the atoms. By contrast, the usual focusing or collimation techniques for light beams and most particle beams is restricted to selection by apertures or conservative forces that preserve the phase space density of atoms in the beam.

This velocity compression at low intensity in one dimension can be easily estimated for two-level atoms to be about $v_c/v_D = \sqrt{\gamma/\omega_r} \equiv \sqrt{1/\varepsilon}$. Here v_D is the velocity associated with the Doppler limit for laser cooling discussed above: $v_D = \sqrt{\hbar\gamma/2M}$. For Rb, v_D = 12 cm s^{-1}, $v_c = \gamma/k \simeq 4.6$ m s^{-1}, $\omega_r \simeq 2\pi \times 3.8$ kHz, and $1/\varepsilon \simeq 1600$. (The parameter ε characterizes optical forces on atoms.) Including two transverse directions along with the longitudinal slowing and cooling discussed above, the decrease in three-dimensional 3-D phase space volume for laser cooling of an Rb atomic beam from the momentum contribution alone •can exceed 10^6. Clearly optical techniques can create atomic beams enormously more times intense than ordinary thermal beams and also many orders of magnitude brighter.

Q8

3.2.4 Experiments in Three-dimensional Optical Molasses

By using three intersecting orthogonal pairs of oppositely directed beams, the movement of atoms in the intersection region can be severely restricted in all 3-D, and many atoms can thereby be collected and cooled in a small volume.

Even though atoms can be collected and cooled in the intersection region, it is important to stress that this is *not* a trap (see Sect. 4 below), that is, atoms that wander away from the center experience no force directing them back. They are allowed to diffuse freely and even escape, as long as there is enough time for their very slow diffusive movement to allow them to reach the edge of the region of intersection of the laser beams. Since the atomic velocities are randomized during the damping time $M/\beta = 2/\omega_r$, atoms execute a random walk in position space with a step size of $2v_D/\omega_r = \lambda/(\pi\sqrt{2\varepsilon}) \cong$ few μm. To diffuse a distance of 1 cm requires about 10^7 steps or about 30 s [13, 14].

In 1985, the group at Bell Labs was the first to observe 3-D OM [11]. Preliminary measurements of the average kinetic energy of the atoms were done by blinking off the laser beams for a fixed interval. Comparison of the brightness of the fluorescence before and after the turnoff was used to calculate the fraction of atoms that left the region while it was in the dark. The dependence of this fraction on the duration of the dark interval was used to estimate the velocity distribution and hence the temperature. This method, which is usually referred to as *release and recapture*, is specifically designed to measure the temperature of the atoms, since the usual way of measuring temperatures cannot be applied to an atomic cloud of a few million atoms. The result was consistent with T_D as calculated from the Doppler theory, as described in Sect. 3.2.2.

Later a more sensitive ballistic technique was devised at NIST that showed the astounding result that the temperature of the atoms in OM was very much lower than T_D [15]. These experiments also found that OM was less sensitive to perturbations and more tolerant of alignment errors than was predicted by Doppler theory. For example, if the intensities of the two counterpropagating laser beams forming

an OM were unequal, then the force on the atoms at rest would not vanish, but the force on the atoms with some nonzero drift velocity *would* vanish. This drift velocity can be easily calculated by using unequal intensities s_{0+} and s_{0-}, to derive an analog of Eq. (13). Thus, atoms would drift out of an OM, and the calculated rate would be much faster than observed by deliberately unbalancing the beams in the experiments [16].

3.3 Cooling Below the Doppler Limit

3.3.1 Introduction

It was an enormous surprise to observe that the ballistically measured temperature of the Na atoms was as much as 10 times *lower* than $T_D = 240\ \mu K$ [15], the temperature minimum calculated from theory. This breaching of the Doppler limit forced the development of an entirely new picture of OM that accounts for the fact that in 3-D, a two-level picture of atomic structure is inadequate. The multilevel structure of atomic states, and optical pumping among these sublevels, must be considered in the description of 3-D OM.

In response to these surprising measurements of temperatures below T_D, two groups developed a model of laser cooling that could explain the lower temperatures [17, 18]. The key feature of this model that distinguishes it from the earlier picture is the inclusion of the multiplicity of sublevels that make up an atomic state (e.g., Zeeman and hfs). The dynamics of optically pumping the moving atoms among these sublevels provides the new mechanism for producing ultralow temperatures [19].

The dominant feature of these models is the nonadiabatic response of moving atoms to the light field. Atoms at rest in a steady state have ground-state orientations caused by optical pumping processes that distribute the populations over the different ground-state sublevels. In the presence of polarization gradients, these orientations reflect the local light field. In the low-light-intensity regime, the orientation of stationary atoms is completely determined by the ground-state distribution; the optical coherences and the excited-state population follow the ground-state distribution adiabatically.

For atoms moving in a light field that varies in space, optical pumping acts to adjust the atomic orientation to the changing conditions of the light field. In a weak pumping process, the orientation of moving atoms always lags behind the orientation that would exist for stationary atoms. It is this phenomenon of nonadiabatic following that is the essential feature of the new cooling process.

Production of spatially dependent optical pumping processes can be achieved in several different ways. As an example, consider two counterpropagating laser beams that have orthogonal polarizations, as discussed below. The superposition of the two beams results in a light field having a polarization that varies on the wavelength scale along the direction of the laser beams. Laser cooling by such a light field is called polarization gradient cooling. In a 3-D OM, the transverse wave character of light requires that the light field always has polarization gradients.

3.3.2 Linear ⊥ Linear Polarization Gradient Cooling

One of the most instructive models for discussion of sub-Doppler laser cooling was introduced in Ref. [17] and very well described in Ref. [19]. If the polarizations of two counterpropagating laser beams are identical, the two beams interfere

and produce a standing wave. When the two beams have orthogonal linear polarizations (same frequency ω_l) with their $\hat{\mathcal{E}}$ vectors perpendicular (e.g., $\hat{x}$ and $\hat{y}$), the configuration is called lin $\perp$ lin or lin-perp-lin. Then the total field is the sum of the two counterpropagating beams given by

$$\begin{aligned}\vec{\mathcal{E}} &= \mathcal{E}_0\,\hat{x}\cos(\omega_l t - kz) + \mathcal{E}_0\hat{y}\cos(\omega_l t + kz)\\ &= \mathcal{E}_0[(\hat{x}+\hat{y})\cos\omega_l t\cos kz\\ &\quad + (\hat{x}-\hat{y})\sin\omega_l t\sin kz]. \qquad (14)\end{aligned}$$

At the origin, where $z = 0$, this becomes

$$\vec{\mathcal{E}} = \mathcal{E}_0(\hat{x}+\hat{y})\cos\omega_l t, \qquad (15)$$

which corresponds to linearly polarized light at an angle $+\pi/4$ to the x-axis. The amplitude of this field is $\sqrt{2}\mathcal{E}_0$. Similarly, for $z = \lambda/4$, where $kz = \pi/2$, the field is also linearly polarized but at an angle $-\pi/4$ to the x-axis.

Between these two points, at $z = \lambda/8$, where $kz = \pi/4$, the total field is

$$\begin{aligned}\vec{\mathcal{E}} = \mathcal{E}_0\Big[&\hat{x}\sin\Big(\omega_l t + \frac{\pi}{4}\Big)\\ &- \hat{y}\cos\Big(\omega_l t + \frac{\pi}{4}\Big)\Big]. \qquad (16)\end{aligned}$$

Since the $\hat{x}$ and $\hat{y}$ components have sine and cosine temporal dependence, they are $\pi/2$ out of phase, and so Eq. (16) represents circularly polarized light rotating about the z-axis in the negative sense. Similarly, at $z = 3\lambda/8$ where $kz = 3\pi/4$, the polarization is circular but in the positive sense. Thus, in this lin $\perp$ lin scheme the polarization cycles from linear to circular to orthogonal linear to opposite circular in the space of only half a wavelength of light, as shown in Fig. 6. It truly has a very strong polarization gradient.

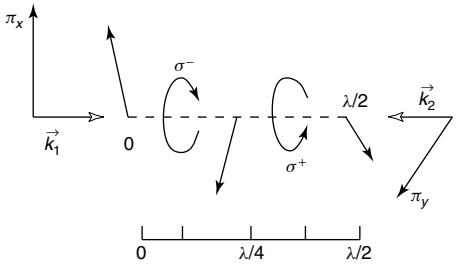

Fig. 6 Polarization gradient field for the lin $\perp$ lin configuration

Since the coupling of the different states of multilevel atoms to the light field depends on its polarization, atoms moving in a polarization gradient will be coupled differently at different positions, and this will have important consequences for laser cooling. For the $J_g = 1/2 \rightarrow J_e = 3/2$ transition (one of the simplest transitions that show sub-Doppler cooling [20]), the optical pumping process in purely σ^+ light drives the ground-state population to the $M_g = +1/2$ sublevel. This optical pumping occurs because absorption always produces $\Delta M = +1$ transitions, whereas the subsequent spontaneous emission produces $\Delta M = \pm 1,\ 0$. Thus, the average $\Delta M \geq 0$ for each scattering event. For σ^--light, the population is pumped toward the $M_g = -1/2$ sublevel. Thus, atoms traveling through only a half wavelength in the light field, need to readjust their population completely from $M_g = +1/2$ to $M_g = -1/2$ and back again.

The interaction between nearly resonant light and atoms not only drives transitions between atomic energy levels but also shifts their energies. This light shift of the atomic energy levels, discussed in Sect. 2.2, plays a crucial role in this scheme of sub-Doppler cooling, and the changing polarization has a strong influence on the light shifts. In the low-intensity limit of two laser beams, each of intensity $s_0 I_s$, the

light shifts ΔE_g of the ground magnetic substates are given by a slight variation of the approximation to Eq. (5) that accounts for the multilevel structure of the atoms. We write

$$\Delta E_g = \frac{\hbar s_0 C_{ge}^2 \gamma^2}{8\delta}, \qquad (17)$$

where C_{ge} is the Clebsch–Gordan coefficient that describes the coupling between the particular levels of the atom and the light field.

In the present case of orthogonal linear polarizations and $J = 1/2 \rightarrow 3/2$, the light shift for the magnetic substate $M_g = 1/2$ is three times larger than that of the $M_g = -1/2$ substate when the light field is completely σ^+. On the other hand, when an atom moves to a place where the light field is σ^-, the shift of $M_g = -1/2$ is three times larger. So, in this case, the optical pumping discussed above causes a larger population to be there •in the state with the larger light shift. This is generally true for any transition $J_g \rightarrow J_e = J_g + 1$. A schematic diagram showing the populations and light shifts for this particular case of negative detuning is illustrated in Fig. 7.

Q9

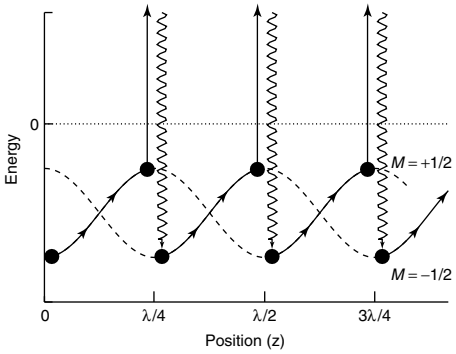

Fig. 7 The spatial dependence of the light shifts of the ground-state sublevels of the $J = 1/2 \Leftrightarrow 3/2$ transition for the case of lin ⊥ lin polarization configuration. The arrows show the path followed by atoms being cooled in this arrangement. Atoms starting at $z = 0$ in the $M_g = +1/2$ sublevel must climb the potential hill as they approach the $z = \lambda/4$ point where the light becomes σ^- polarized, and they are optically pumped to the $M_g = -1/2$ sublevel. Then they must begin climbing another hill toward the $z = \lambda/2$ point where the light is σ^+ polarized and they are optically pumped back to the $M_g = +1/2$ sublevel. The process repeats until the atomic kinetic energy is too small to climb the next hill. Each optical pumping event results in the absorption of light at a frequency lower than emission, thus dissipating energy to the radiation field

3.3.3 Origin of the Damping Force

To discuss the origin of the cooling process in this polarization gradient scheme, consider atoms with a velocity v at a position where the light is σ^+-polarized, as shown at the lower left of Fig. 7. The light optically pumps such atoms to the strongly negative light-shifted $M_g = +1/2$ state. In moving through the light field, atoms must increase their potential energy (climb a hill) because the polarization of the light is changing and the state $M_g = 1/2$ becomes less strongly coupled to the light field. After traveling a distance $\lambda/4$, atoms arrive at a position where the light field is σ^--polarized, and are optically pumped to $M_g = -1/2$, which is now lower than the $M_g = 1/2$ state. Again, the moving atoms are at the bottom of a hill and start to climb. In climbing the hills, the kinetic energy is converted to potential energy, and in the optical pumping process, the potential energy is radiated away because the spontaneous emission is at a higher frequency than the absorption (see Fig. 7). Thus, atoms seem to be always climbing hills and losing energy in the process. This process brings to mind a Greek myth, and is thus called ''Sisyphus laser cooling''.

The cooling process described above is effective over a limited range of atomic velocities. The force is maximum for atoms that undergo one optical pumping process while traveling over a distance $\lambda/4$. Slower atoms will not reach the hilltop before the pumping process occurs and faster atoms will travel a longer distance before being pumped toward the other sublevel, so $\Delta E/\Delta z$ is smaller. In both cases, the energy loss is smaller and therefore the cooling process less efficient. Nevertheless, the damping constant β for this process is much larger than for Doppler cooling, and therefore the final steady state temperature is lower [17, 19].

In the experiments of Ref. [21], the temperature was measured in a 3-D molasses under various configurations of the polarization. Temperatures were measured by a ballistic technique, in which the flight time of the released atoms was measured as they fell through a probe a few centimeters below the molasses region. The lowest temperature obtained was 3 μK, which is a factor 40 below the Doppler temperature and a factor 15 above the recoil temperature of Cs.

3.3.4 The Limits of Sisyphus Laser Cooling

The extension of the kind of thinking about cooling limits in the case of Doppler cooling to the case of the sub-Doppler processes must be done with some care, because a naive application of similar ideas would lead to an arbitrarily low final temperature. In the derivation in Sect. 3.2.2, it is explicitly assumed that each scattering event changes the atomic momentum p by an amount that is a small fraction of p and this clearly fails when the velocity is reduced to the region of $v_r \equiv \hbar k/M$.

This limitation of the minimum steady state value of the average kinetic energy to a few times $E_r \equiv k_B T_r/2 = M v_r^2/2$ is intuitively comforting for two reasons. First, one might expect that the last spontaneous emission in a cooling process would leave atoms with a residual momentum of the order of $\hbar k$, since there is no control over its direction. Thus, the randomness associated with this would put a lower limit of $v_{min} \sim v_r$ on such cooling. Second, the polarization gradient cooling mechanism described above requires that atoms be localizable within the scale of $\sim \lambda/2\pi$ in order to be subject to only a single polarization in the spatially inhomogeneous light field. The uncertainty principle then requires that these atoms have a momentum spread of at least $\hbar k$.

The recoil limit discussed here has been surpassed by evaporative cooling of trapped atoms [22] and two different optical cooling methods, neither of which can be described in simple notions. One of these uses optical pumping into a velocity-selective dark state [23]. The other one uses carefully chosen, counterpropagating, laser pulses to induce velocity-selective Raman transitions, and is called *Raman cooling* [24].

4 Traps for Neutral Atoms

In order to confine any object, it is necessary to exchange kinetic for potential energy in the trapping field, and in neutral atom traps, the potential energy must be stored as internal atomic energy. Thus, practical traps for ground-state neutral atoms are necessarily very shallow compared with thermal energy because the energy-level shifts that result from convenient size fields are typically considerably smaller than $k_B T$ for $T = 1$ K. Neutral atom trapping therefore depends

on substantial cooling of a thermal atomic sample, and is often connected with the cooling process. In most practical cases, atoms are loaded from magneto-optical traps (MOTs) in which they have been efficiently accumulated and cooled to mK temperatures (see Sect. 4.3), or from optical molasses, in which they have been optically cooled to μK temperatures (see Sect. 3.2).

The small depth of typical neutral atom traps dictates stringent vacuum requirements because an atom cannot remain trapped after a collision with a thermal energy background gas molecule. Since these atoms are vulnerable targets for thermal energy background gas, the mean free time between collisions *must* exceed the desired trapping time. The cross section for destructive collisions is quite large because even a gentle collision (i.e., large impact parameter) can impart enough energy to eject an atom from a trap. At pressure P sufficiently low to be of practical interest, the trapping time is $\sim (10^{-8}/P)$ s, where P is in Torr.

4.1 Dipole Force Optical Traps

4.1.1 Single-beam Optical Traps for Two-level Atoms

The simplest imaginable optical trap consists of a single, strongly focused Gaussian laser beam (see Fig. 8) [25, 26] whose intensity at the focus varies transversely with r as

$$I(r) = I_0 e^{-2r^2/w_0^2}, \qquad (18)$$

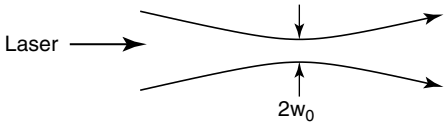

Fig. 8 A single focused laser beam produces the simplest type of optical trap

where w_0 is the beam waist size. Such a trap has a well-studied and important macroscopic classical analog in a phenomenon called *optical tweezers* [27–29].

With the laser light tuned below resonance ($\delta < 0$), the ground-state light shift is negative everywhere, but largest at the center of the Gaussian beam waist. Ground-state atoms, therefore, experience a force attracting them toward this center, given by the gradient of the light shift, which is found from Eq. (5), and for $\delta/\gamma \gg s_0$ is given by Eq. (6). For the Gaussian beam, this transverse force at the waist is harmonic for small r and is given by

$$F \simeq \frac{\hbar\gamma^2}{4\delta}\frac{I_0}{I_s}\frac{r}{w_0^2}e^{-2r^2/w_0^2}. \qquad (19)$$

In the longitudinal direction, there is also an attractive force but it is more complicated and depends on the details of the focusing. Thus, this trap produces an attractive force on the atoms in three dimensions.

Although it may appear that the trap does not confine atoms longitudinally because of the radiation pressure along the laser beam direction, careful choice of the laser parameters can indeed produce trapping in 3-D. This can be accomplished because the radiation pressure force decreases as $1/\delta^2$ (see Eqs. 2 and 3), but by contrast, the light shift and hence the dipole force decreases only as $1/\delta$ for $\delta \gg \Omega$ (see Eq. 5). If $|\delta|$ is chosen to be sufficiently large, atoms spend very little time in the untrapped (actually repelled), excited state because its population is proportional to $1/\delta^2$. Thus, a sufficiently large value of $|\delta|$ produces longitudinal confinement and also maintains the atomic population primarily in the trapped ground state.

The first optical trap was demonstrated in Na with light detuned below the D-lines [26]. With 220 mW of dye laser light

tuned about 650 GHz below the atomic transition and focused to an $\sim$10 μm waist, the trap depth was about $15\hbar\gamma$ corresponding to 7 mK.

Single-beam dipole force traps can be made with the light detuned by a significant fraction of its frequency from the atomic transition. Such a far-off-resonance trap (FORT) has been developed for Rb atoms using light detuned by nearly 10% to the red of the D_1 transition at $\lambda = 795$ nm [30]. Between 0.5 and 1 W of power was focused to a spot about 10 μm in size, resulting in a trap 6 mK deep where the light-scattering rate was only a few hundreds per second. The trap lifetime was more than half a second.

There is a qualitative difference when the trapping light is detuned by a large fraction of the optical frequency. In one such case, Nd : YAG light at $\lambda = 1064$ nm was used to trap Na whose nearest transition is at $\lambda = 596$ nm [31]. In a more extreme case, a trap using $\lambda = 10.6$ μm light from a CO_2 laser has been used to trap Cs whose optical transition is at a frequency $\sim$12 times higher ($\lambda = 852$ nm) [32]. For such large values of $|\delta|$, calculations of the trapping force cannot exploit the rotating wave approximations as was done for Eqs. (4) and (5), and the atomic behavior is similar to that in a DC field. It is important to remember that for an electrostatic trap Earnshaw's theorem precludes a field maximum, but that in this case there is indeed a local 3-D intensity maximum of the focused light because it is not a static field.

4.1.2 **Blue-detuned Optical Traps**

One of the principal disadvantages of the optical traps discussed above is that the negative detuning attracts atoms to the region of highest light intensity. This may result in significant spontaneous emission unless the detuning is a large fraction of the optical frequency such as the Nd : YAG laser trap [31] or the CO_2 laser trap [32]. More important in some cases is that the trap relies on Stark shifting of the atomic energy levels by an amount equal to the trap depth, and this severely compromises the capabilities for precision spectroscopy in a trap [33].

Attracting atoms to the region of *lowest* intensity would ameliorate both these concerns, but such a trap requires positive detuning (blue), and an optical configuration having a dark central region. One of the first experimental efforts at a blue detuned trap used the repulsive dipole force to support Na atoms that were otherwise confined by gravity in an optical "cup" [34]. Two rather flat, parallel beams detuned by 25% of the atomic resonance frequency were directed horizontally and oriented to form a V-shaped trough. Their Gaussian beam waists formed a region $\simeq$1 mm long where the potential was deepest, and hence provided confinement along their propagation direction as shown in Fig. 9. The beams were the $\lambda = 514$ nm and $\lambda = 488$ nm from an argon laser, and

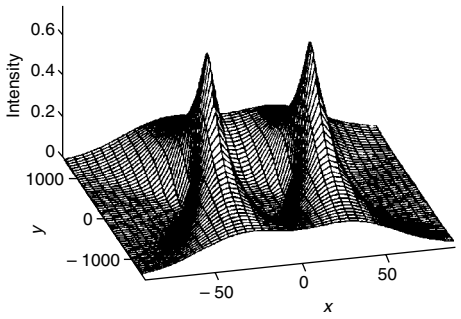

Fig. 9 The light intensity experienced by an atom located in a plane 30 μm above the beam waists of two quasi-focused sheets of light traveling parallel and arranged to form a V-shaped trough. The *x* and *y* dimensions are in μm (figure taken from Davidson, N., Lee, H. J., Adams, C. S., Kasevich, M., Chu, S. (**1995**), *Phys. Rev. Lett.* **74**, 1311–1314)

the choice of the two frequencies was not simply to exploit the full power of the multiline Ar laser, but also to avoid the spatial interference that would result from the use of a single frequency.

Obviously, a hollow laser beam would also satisfy the requirement for a blue-detuned trap, but conventional textbook wisdom shows that such a beam is not an eigenmode of a laser resonator [35]. Some lasers can make hollow beams, but these are illusions because they consist of rapid oscillations between the TEM_{01} and TEM_{10} modes of the cavity. Nevertheless, Maxwell's equations permit the propagation of such beams, and in the recent past there have been studies of the LaGuerre–Gaussian modes that constitute them [36–38]. The several ways of generating such hollow beams have been tried by many experimental groups and include phase and amplitude holograms, hollow waveguides, axicons or related cylindrical prisms, stressing fibers, and simply mixing the TEM_{01} and TEM_{10} modes with appropriate cylindrical lenses.

An interesting experiment has been performed using the ideas of Sisyphus cooling (see Sect. 3.3.3●) with evanescent waves combined with a hollow beam formed with an axicon [39]. In the previously reported experiments with atoms bouncing under gravity from an evanescent wave field [40, 41], they were usually lost to horizontal motion for several reasons, including slight tilting of the surface, surface roughness, horizontal motion associated with their residual motion, and horizontal ejection by the Gaussian profile of the evanescent wave laser beam. The authors of Ref. [39] simply confined their atoms in the horizontal direction by surrounding them with a wall of blue-detuned light in the form of a vertical hollow beam. Their gravito-optical surface trap cooled Cs atoms to $\simeq 3\,\mu K$ at a density of $\simeq 3 \times 10^{10}/cm^3$ in a sample whose $1/e$ height in the gravitational field was only 19 μm. Simple ballistics gives a frequency of 450 bounces per second, and the ≃6-s lifetime (limited only by background gas collisions) corresponds to several thousand bounces. However, at such low energies, the deBroglie wavelength of the atoms is $\simeq 1/4\,\mu m$, and the atomic motion is no longer accurately described classically, but requires deBroglie wave methods.

Q10

4.2 Magnetic Traps

4.2.1 Introduction

Magnetic trapping of neutral atoms is well suited for use in very many areas, including high-resolution spectroscopy, collision studies, Bose–Einstein condensation (BEC), and atom optics. Although ion trapping, laser cooling of trapped ions, and trapped ion spectroscopy were known for many years [42], it was only in 1985 that neutral atoms were first trapped [43]. Such experiments offer the capability of the spectroscopic ideal of an isolated atom at rest, in the dark, available for interaction with electromagnetic field probes.

Because trapping requires the exchange of kinetic energy for potential energy, the atomic energy levels will necessarily shift as the atoms move in the trap. These shifts can severely affect the precision of spectroscopic measurements. Since one of the potential applications of trapped atoms is in high-resolution spectroscopy, such inevitable shifts must be carefully considered.

4.2.2 Magnetic Confinement

The Stern–Gerlach experiment in 1924 first demonstrated the mechanical action of inhomogeneous magnetic fields on

neutral atoms having magnetic moments, and the basic phenomenon was subsequently developed and refined. An atom with a magnetic moment $\vec{\mu}$ can be confined by an inhomogeneous magnetic field because of an interaction between the moment and the field. This produces a force given by

$$\vec{F} = \vec{\nabla}(\vec{\mu} \cdot \vec{B}) \tag{20}$$

since $E = -\vec{\mu} \cdot \vec{B}$. Several different magnetic traps with varying geometries that exploit the force of Eq. (20) have been studied in some detail in the literature. The general features of the magnetic fields of a large class of possible traps has been presented [44].

W. Paul originally suggested a quadrupole trap composed of two identical coils carrying opposite currents (see Fig. 10). This trap clearly has a single center in which the field is zero, and is the simplest of all possible magnetic traps. When the coils are separated by 1.25 times their radius, such a trap has equal depth in the radial (x-y plane) and longitudinal (z-axis) directions [44]. Its experimental simplicity makes it most attractive, both because of ease of construction and of optical access to the interior. Such a trap was used in the first neutral atom trapping experiments at NIST on laser-cooled Na atoms for times exceeding 1 s, and that time was limited only by background gas pressure [43].

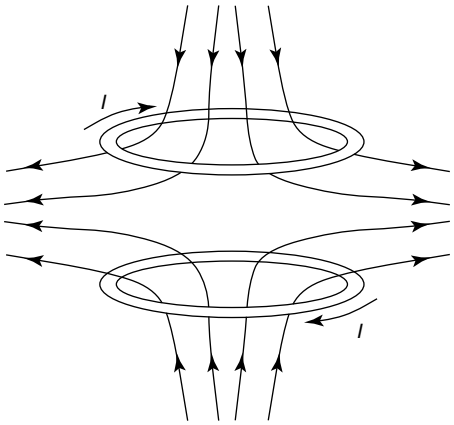

Fig. 10 Schematic diagram of the coil configuration used in the quadrupole trap and the resultant magnetic field lines. Because the currents in the two coils are in opposite directions, there is a $|\vec{B}| = 0$ point at the center

The magnitude of the field is zero at the center of this trap, and increases in all directions as

$$B = \nabla B\sqrt{\rho^2 + 4z^2}, \tag{21}$$

where $\rho^2 \equiv x^2 + y^2$ and the field gradient is constant (see Ref. [44]). The field gradient is constant along any line through the origin, but has different values in different polar directions because of the '4' in Eq. (21). Therefore, the force of Eq. (20) that confines the atoms in the trap is neither harmonic nor central, and orbital angular momentum is not conserved.

The requisite field for the quadrupole trap can also be provided in two dimensions by four straight currents as indicated in Fig. 11. The field is translationally invariant along the direction parallel to the currents, so a trap cannot be made this way without additional fields. These are provided by end coils that close the trap, as shown.

Although there are very many different kinds of magnetic traps for neutral particles, this particular one has played a special

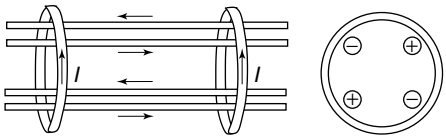

Fig. 11 The Ioffe trap has four straight current elements that form a linear quadrupole field. The axial confinement is accomplished with end coils as shown. These fields can be achieved with many different current configurations as long as the geometry is preserved

role. There are certain conditions required for trapped atoms not to be ejected in a region of zero field such as occurs at the center of a quadrupole trap (see Sects. 4.2.3 and 4.2.4). This problem is not easily cured; the Ioffe trap has been used in many of the BEC experiments because it has $|\vec{B}| \neq 0$ everywhere.

4.2.3 Classical Motion of Atoms in a Quadrupole Trap

Because of the dependence of the trapping force on the angle between the field and the atomic moment (see Eq. 20), the orientation of the magnetic moment with respect to the field must be preserved as the atoms move about in the trap. Otherwise, the atoms may be ejected instead of being confined by the fields of the trap. This requires velocities low enough to ensure that the interaction between the atomic moment $\vec{\mu}$ and the field $\vec{B}$ is adiabatic especially when the atom's path passes through a region where the field magnitude is small and therefore the energy separation between the trapping and nontrapping states is small. This is especially critical at the low temperatures of the BEC experiments. Therefore energy considerations that focus only on the trap depth are not sufficient to determine the stability of a neutral atom trap; orbit and/or quantum state calculations and their consequences must also be considered.

For the two-coil quadrupole magnetic trap of Fig. 10, stable circular orbits of radius ρ_1 in the $z = 0$ plane can be found classically by setting $\mu \nabla B = Mv^2/\rho_1$, so that $v = \sqrt{\rho_1 a}$, where $a \equiv \mu \nabla B/M$ is the centripetal acceleration supplied by the field gradient (cylindrical coordinates are appropriate). Such orbits have an angular frequency of $\omega_T = \sqrt{a/\rho_1}$. For traps of a few centimeter size and a few hundred Gauss depth, $a \sim 250\ \mathrm{m\ s^{-2}}$, and the fastest trappable atoms in circular orbits have $v_{\max} \sim 1\ \mathrm{m\ s^{-1}}$ so $\omega_T/2\pi \sim 20$ Hz. Because of the anharmonicity of the potential, the orbital frequencies depend on the orbit size, but in general, atoms in lower-energy orbits have higher frequencies.

For the quadrupole trap to work, the atomic magnetic moments must be oriented with $\vec{\mu} \cdot \vec{B} < 0$ so that they are repelled from regions of strong fields. This orientation must be preserved while the atoms move around in the trap even though the trap fields change directions in a very complicated way. The condition for adiabatic motion can be written as $\omega_Z \gg |\mathrm{d}B/\mathrm{d}t|/B$, where $\omega_Z = \mu B/\hbar$ is the Larmor precession rate in the field.

Since $v/\rho_1 = v \nabla B/B = |\mathrm{d}B/\mathrm{d}t|/B$ for a uniform field gradient, the adiabaticity condition is

$$\omega_Z \gg \omega_T. \tag{22}$$

More general orbits must satisfy a similar condition. For the two-coil quadrupole trap, the adiabaticity condition can be easily calculated. Using $v = \sqrt{\rho_1 a}$ for circular orbits in the $z = 0$ plane, the adiabatic condition for a practical trap ($\nabla B \sim 1$ T/m) requires $\rho_1 \gg (\hbar^2/M^2 a)^{1/3} \sim 1\ \mu$m as well as $v \gg (\hbar a/M)^{1/3} \sim 1\ \mathrm{cm\ s^{-1}}$. Note that violation of these conditions (i.e., $v \sim 1\ \mathrm{cm\ s^{-1}}$ in a trap with $\nabla B \sim 1$ T/m) results in the onset of quantum dynamics for the motion (deBroglie wavelength $\approx$ orbit size).

Since the nonadiabatic region of the trap is so small (less than $10^{-18}\ \mathrm{m^3}$ compared with typical sizes of $\sim$2 cm, corresponding to $10^{-5}\ \mathrm{m^3}$), nearly all the orbits of most atoms are restricted to regions where they are adiabatic. Therefore, most of such laser-cooled atoms stay trapped for

many thousands of orbits corresponding to several minutes. At laboratory vacuum chamber pressures of typically 10^{-10} torr, the mean free time between collisions that can eject trapped atoms is ~2 min, so the transitions caused by nonadiabatic motion are not likely to be observable in atoms that are optically cooled.

4.2.4 Quantum Motion in a Trap

Since laser and evaporative cooling have the capability to cool atoms to energies where their deBroglie wavelengths are on the scale of the orbit size, the motional dynamics must be described in terms of quantum mechanical variables and suitable wave functions. Quantization of the motion leads to discrete bound states within the trap having $\vec{\mu} \cdot \vec{B} < 0$, and also a continuum of unbound states having $\vec{\mu} \cdot \vec{B}$ with opposite sign.

Studying the behavior of extremely slow (cold) atoms in the two-coil quadrupole trap begins with a heuristic quantization of the orbital angular momentum using $Mr^2\omega_T = n\hbar$ for circular orbits. The energy levels are then given by

$$E_n = \frac{3}{2} E_1 n^{2/3}, \quad \text{where}$$
$$E_1 = (Ma^2\hbar^2)^{1/3} \sim h \times 5\ \text{kHz}, \quad (23)$$

For velocities of optically cooled atoms of a few cm s^{-1}, $n \sim 10 - 100$. It is readily found that $\omega_Z = n\omega_T$, so that the adiabatic condition of Eq. (22) is satisfied only for $n \gg 1$.

These large-n bound states have small matrix elements coupling them to the unbound continuum states [45]. This can be understood classically since they spend most of their time in a stronger field, and thus satisfy the condition of adiabaticity of the orbital motion relative to the Larmor precession. In this case, the separation of the rapid precession from the slower orbital motion is reminiscent of the Born–Oppenheimer approximation for molecules.

On the other hand, the small-n states, whose orbits are confined to a region near the origin where the field is small, have much larger coupling to the continuum states. Thus, they are rapidly ejected from the trap. The transitions to unbound states resulting from the coupling of the motion with the trapping fields are called *Majorana spin flips*, and effectively constitute a "hole" at the bottom of the trap. The evaporative cooling process used to produce very cold, dense samples reduces the average total energy of the trapped atoms sufficiently that the orbits are confined to regions near the origin and so, such losses dominate [44, 45].

There have been different solutions to this problem of Majorana losses for confinement of ultracold atoms for the BEC experiments. In the JILA-experiment, the hole was rotated by rotating the magnetic field, and thus, the atoms do not spend sufficient time in the hole to make a spin flip. In the MIT experiment, the hole was plugged by using a focused laser beam tuned to the blue side of atomic resonance, which expelled the atoms from the center of the magnetic trap. In the Rice experiment, the atoms were trapped in an Ioffe trap, which has a nonzero field minimum. Most BEC experiments are now using the Ioffe trap solution.

4.3 Magneto-optical Traps

4.3.1 Introduction

The most widely used trap for neutral atoms is a hybrid employing both optical and magnetic fields to make a magneto-optical trap (MOT), first demonstrated in

1987 [46]. The operation of an MOT depends on both inhomogeneous magnetic fields and radiative selection rules to exploit both optical pumping and the strong radiative force [46, 47]. The radiative interaction provides cooling that helps in loading the trap and enables very easy operation. MOT is a very robust trap that does not depend on precise balancing of the counterpropagating laser beams or on a very high degree of polarization.

The magnetic field gradients are modest and have the convenient feature that the configuration is the same as the quadrupole magnetic traps discussed in Sect. 4.2.2. Appropriate fields can readily be achieved with simple, air-cooled coils. The trap is easy to construct because it can be operated with a room-temperature cell in which alkali atoms are captured from the vapor. Furthermore, low-cost diode lasers can be used to produce the light appropriate for many atoms, so the MOT has become one of the least expensive ways to make atomic samples with temperatures below 1 mK.

Trapping in an MOT works by optical pumping of slowly moving atoms in a linearly inhomogeneous magnetic field $B = B(z)$ (see Eq. 21), such as that formed by a magnetic quadrupole field. Atomic transitions with the simple scheme of $J_g = 0 \rightarrow J_e = 1$ have three Zeeman components in a magnetic field, excited by each of three polarizations, whose frequencies tune with the field (and therefore with position) as shown in Fig. 12 for 1-D. Two counterpropagating laser beams of opposite circular polarization, each detuned below the zero-field atomic resonance by δ, are incident as shown.

Because of the Zeeman shift, the excited state $M_e = +1$ is shifted up for $B > 0$, whereas the state with $M_e = -1$ is shifted down. At position z' in Fig. 12,

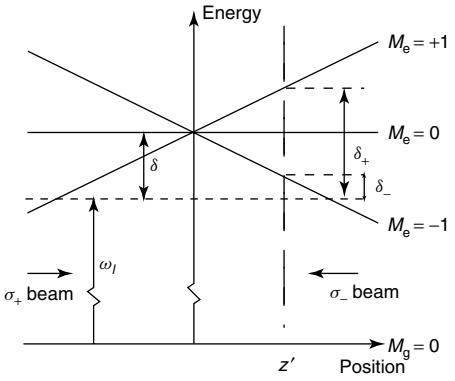

Fig. 12 Arrangement for an MOT in 1-D. The horizontal dashed line represents the laser frequency seen by an atom at rest in the center of the trap. Because of the Zeeman shifts of the atomic transition frequencies in the inhomogeneous magnetic field, atoms at $z = z'$ are closer to resonance with the σ^- laser beam than with the σ^+ beam, and are therefore driven toward the center of the trap

the magnetic field, therefore, tunes the $\Delta M = -1$ transition closer to resonance and the $\Delta M = +1$ transition further out of resonance. If the polarization of the laser beam incident from the right is chosen to be σ^- and correspondingly σ^+ for the other beam, then more light is scattered from the σ^- beam than from the σ^+ beam. Thus, the atoms are driven toward the center of the trap where the magnetic field is zero. On the other side of the center of the trap, the roles of the $M_e = \pm 1$ states are reversed and now more light is scattered from the σ^+ beam, again driving the atoms toward the center.

So far, the discussion has been limited to the motion of atoms in 1-D. However, the MOT scheme can easily be extended to 3-D by using six instead of two laser beams. Furthermore, even though very few atomic species have transitions as simple as $J_g = 0 \rightarrow J_e = 1$, the scheme works for any $J_g \rightarrow J_e = J_g + 1$ transition. Atoms that scatter mainly from the σ^+

laser beam will be optically pumped toward the $M_g = +J_g$ substate, which forms a closed system with the $M_e = +J_e$ substate.

4.3.2 Cooling and Compressing Atoms in an MOT

For a description of the motion of atoms in an MOT, consider the radiative force in the low intensity limit (see Eqs. 2 and 3). The total force on the atoms is given by $\vec{F} = \vec{F}_+ + \vec{F}_-$, where $\vec{F}_\pm$ can be found from Eqs. (2) and (3), and the detuning $\delta_\pm$ for each laser beam is given by $\delta_\pm = \delta \mp \vec{k} \cdot \vec{v} \pm \mu' B/\hbar$. Here, $\mu' \equiv (g_e M_e - g_g M_g)\mu_B$ is the effective magnetic moment for the transition used. Note that the Doppler shift $\omega_D \equiv -\vec{k} \cdot \vec{v}$ and the Zeeman shift $\omega_Z = \mu' B/\hbar$ both have opposite signs for opposite beams.

The situation is analogous to the velocity damping in an OM from the Doppler effect as discussed in Sec. 3.2, but here the effect also operates in position space, whereas for molasses it operates only in velocity space. Since the laser light is detuned below the atomic resonance in both cases, compression and cooling of the atoms is obtained simultaneously in an MOT.

When both the Doppler and Zeeman shifts are small compared to the detuning δ, the denominator of the force can be expanded as for Eq. (13) and the result becomes

$$\vec{F} = -\beta\vec{v} - \kappa\vec{r}, \qquad (24)$$

where the damping coefficient β is defined in Eq. (13). The spring constant κ arises from the similar dependence of $\vec{F}$ on the Doppler and Zeeman shifts, and is given by $\kappa = \mu' \beta \nabla B/\hbar k$

The force of Eq. (24) leads to damped harmonic motion of the atoms, where the damping rate is given by $\Gamma_{MOT} = \beta/M$ and the oscillation frequency $\omega_{MOT} = \sqrt{\kappa/M}$. For magnetic field gradients $\nabla B \approx 0.1\ \mathrm{T\ m^{-1}}$, the oscillation frequency is typically a few kHz, and this is much smaller than the damping rate that is typically a few hundred kHz. Thus, the motion is overdamped, with a characteristic restoring time to the center of the trap of $2\Gamma_{MOT}/\omega_{MOT}^2 \approx$ several milliseconds for typical values of detuning and intensity of the lasers.

4.3.3 Capturing Atoms in an MOT

Although the approximations that lead to Eq. (24) for force hold for slow atoms near the origin, they do not apply for the capture of fast atoms far from the origin. In the capture process, the Doppler and Zeeman shifts are no longer small compared to the detuning, so the effects of the position and velocity can no longer be disentangled. However, the full expression for the force still applies and the trajectories of the atoms can be calculated by numerical integration of the equation of motion [48].

The capture velocity of an MOT is serendipitously enhanced because atoms traveling across it experience a decreasing magnetic field just as in beam deceleration described in Sect. 3.1. This enables resonance over an extended distance and velocity range because the changing Doppler shift of decelerating atoms can be compensated by the changing Zeeman shift as atoms move in the inhomogeneous magnetic field. Of course, it will work this way only if the field gradient ∇B does not demand an acceleration larger than the maximum acceleration a_{max}. Thus, atoms are subject to the optical force over a distance that can be as long as the trap size, and can therefore be slowed considerably.

The very large velocity capture range v_{cap} of an MOT can be estimated by using $F_{max} = \hbar k \gamma/2$ and choosing a maximum size of a few centimeters for the beam

diameters. Thus, the energy change can be as large as a few K, corresponding to $v_{cap} \sim 100\ m\ s^{-1}$ [47]. The number of atoms in a vapor with velocities below v_{cap} in the Boltzmann distribution scales as v_{cap}^4, and there are enough slow atoms to fall within the large MOT capture range even at room temperature, because a few K includes 10^{-4} of the atoms.

4.3.4 Variations on the MOT Technique

Because of the wide range of applications of this most versatile kind of atom trap, a number of careful studies of its properties have been made [47, 49–56], and several variations have been developed. One of these is designed to overcome the density limits achievable in an MOT. In the simplest picture, loading additional atoms into an MOT produces a higher atomic density because the size of the trapped sample is fixed. However, the density cannot increase without limit as more atoms are added. The atomic density is limited to $\sim 10^{11}\ cm^{-3}$ because the fluorescent light emitted by some trapped atoms is absorbed by others.

One way to overcome this limit is to have much less light in the center of the MOT than at the sides. Simply lowering the laser power is not effective in reducing the fluorescence because it will also reduce the capture rate and trap depth. But those advantageous properties can be preserved while reducing fluorescence from atoms at the center if the light intensity is low only in the center.

The repumping process for the alkali atoms provides an ideal way of implementing this idea [57]. If the repumping light is tailored to have zero intensity at the center, then atoms trapped near the center of the MOT are optically pumped into the ''wrong'' hfs state and stop fluorescing. They drift freely in the ''dark'' at low speed through the center of the MOT until they emerge on the other side, into the region where light of both frequencies is present and begin absorbing again. Then they feel the trapping force and are driven back into the ''dark'' center of the trap. Such an MOT has been operated at MIT [57] with densities close to $10^{12}/cm^3$, and the limitations are now from collisions in the ground state rather than from multiple light scattering and excited-state collisions.

5 Optical Lattices

5.1 Quantum States of Motion

As the techniques of laser cooling advanced from a laboratory curiosity to a tool for new problems, the emphasis shifted from attaining the lowest possible steady state temperatures to the study of elementary processes, especially the quantum mechanical description of the atomic motion. In the completely classical description of laser cooling, atoms were assumed to have a well-defined position and momentum that could be known simultaneously with arbitrary precision. However, when atoms are moving sufficiently slowly that their deBroglie wavelength precludes their localization to less than $\lambda/2\pi$, these descriptions fail and a quantum mechanical description is required. Such exotic behavior for the motion of whole atoms, as opposed to electrons in the atoms, had not been considered before the advent of laser cooling simply because it was too far out of the range of ordinary experiments. A series of experiments in the early 1990s provided dramatic evidence for these new quantum states of motion of neutral atoms, and

led to the debut of deBroglie wave atom optics.

The quantum description of atomic motion requires that the energy of such motion be included in the Hamiltonian. The total Hamiltonian for atoms moving in a light field would then be given by

$$\mathcal{H} = \mathcal{H}_{\text{atom}} + \mathcal{H}_{\text{rad}} + \mathcal{H}_{\text{int}} + \mathcal{H}_{\text{kin}}, \quad (25)$$

where $\mathcal{H}_{\text{atom}}$ describes the motion of the atomic electrons and gives the internal atomic energy levels, $\mathcal{H}_{\text{rad}}$ is the energy of the radiation field and is of no concern here because the field is not quantized, $\mathcal{H}_{\text{int}}$ describes the excitation of atoms by the light field and the concomitant light shifts, and $\mathcal{H}_{\text{kin}}$ is the kinetic energy operator of the motion of the center of mass of the atoms. This Hamiltonian has eigenstates of not only the internal energy levels and the atom-laser interaction that connects them, but also that of the kinetic energy operator $\mathcal{H}_{\text{kin}} \equiv P^2/2M$. These eigenstates will therefore be labeled by quantum numbers of the atomic states as well as the center of mass momentum p. An atom in the ground state, $|g; p\rangle$, has an energy $E_g + p^2/2M$, that can take on a range of values.

Q11 In 1968, V.S. Letokhov [58] •suggested that it is possible to confine atoms in the wavelength-size regions of a standing wave by means of the dipole force that arises from the light shift. This was first accomplished in 1987 in 1-D with an atomic beam traversing an intense standing wave [59]. Since then, the study of atoms confined to wavelength-size potential wells has become an important topic in optical control of atomic motion because it opens up configurations previously accessible only in condensed matter physics using crystals.

The limits of laser cooling discussed in Sect. 3.3.4 suggest that atomic momenta can be reduced to a "few" times $\hbar k$. This means that their deBroglie wavelengths are equal to the optical wavelengths divided by a "few". If the depth of the optical potential wells is high enough to contain such very slow atoms, then their motion in potential wells of size $\lambda/2$ must be described quantum mechanically, since they are confined to a space of size comparable to their deBroglie wavelengths. Thus, they do not oscillate in the sinusoidal wells as classical localizable particles, but instead occupy discrete, quantum mechanical bound states [60], as shown in the lower part of Fig. 13.

The basic ideas of the quantum mechanical motion of particles in a periodic potential were laid out in the 1930s with the Kronig–Penney model and Bloch's theorem, and optical lattices offer important opportunities for their study. For example,

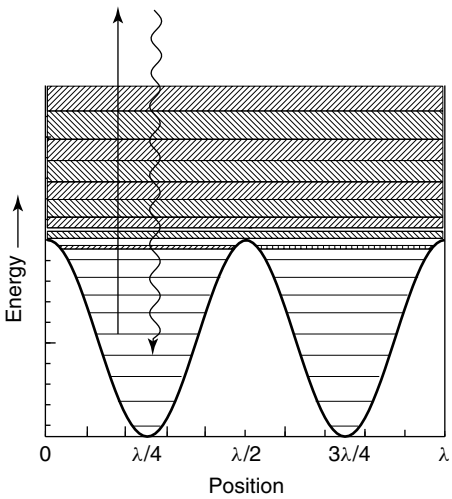

Fig. 13 Energy levels of atoms moving in the periodic potential of the light shift in a standing wave. There are discrete bound states deep in the wells that broaden at higher energy, and become bands separated by forbidden energies above the tops of the wells. Under conditions appropriate to laser cooling, optical pumping among these states favors populating the lowest ones as indicated schematically by the arrows

these lattices can be made essentially free of defects with only moderate care in spatially filtering the laser beams to assure a single transverse mode structure. Furthermore, the shape of the potential is exactly known and does not depend on the effect of the crystal field or the ionic energy level scheme. Finally, the laser parameters can be varied to modify the depth of the potential wells without changing the lattice vectors, and the lattice vectors can be changed independently by redirecting the laser beams. The simplest optical lattice to consider is a 1-D pair of counterpropagating beams of the same polarization, as was used in the first experiment [59].

Of course, such tiny traps are usually very shallow, so loading them requires cooling to the μK regime. Even atoms whose energy exceeds the trap depth must be described as quantum mechanical particles moving in a periodic potential that display energy band structure [60]. Such effects have been observed in very careful experiments.

Because of the transverse nature of light, any mixture of beams with different $\vec{k}$-vectors necessarily produces a spatially periodic, inhomogeneous light field. The importance of the ''egg-crate'' array of potential wells arises because the associated atomic light shifts can easily be comparable to the very low average atomic kinetic energy of laser-cooled atoms. A typical example projected against two dimensions is shown in Fig. 14.

Atoms trapped in wavelength-sized spaces occupy vibrational levels similar to those of molecules. The optical spectrum can show Raman-like sidebands that result from transitions among the quantized vibrational levels [61, 62] as shown in Fig. 15. These quantum states of atomic motion can also be observed by stimulated emission [62, 63] and by direct RF spectroscopy [64, 65].

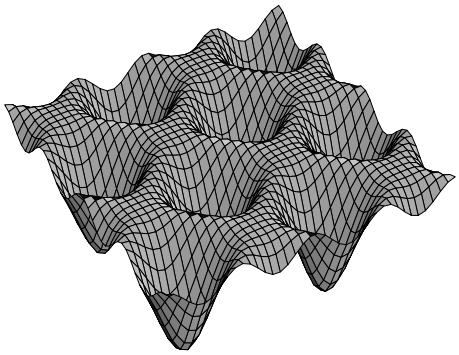

Fig. 14 The ''egg-crate'' potential of an optical lattice shown in two dimensions. The potential wells are separated by $\lambda/2$

5.2 Properties of 3-D Lattices

The name ''optical lattice'' is used rather than optical crystal because the filling fraction of the lattice sites is typically only a few percent (as of 1999). The limit arises because the loading of atoms into the lattice is typically done from a sample of trapped and cooled atoms, such as an MOT for atom collection, followed by an OM for laser cooling. The atomic density in such experiments is limited by collisions and multiple light scattering to a few times 10^{11} cm^{-3}. Since the density of lattice sites of size $\lambda/2$ is a few times 10^{13} cm^{-3}, the filling fraction is necessarily small. With the advent of experiments that load atoms directly into a lattice from a BEC, the filling factor can be increased to 100%, and in some cases it may be possible to load more than one atom per lattice site [66, 67].

In 1993 a very clever scheme was described [68]. It was realized that an n-dimensional lattice could be created by only $n+1$ traveling waves rather than

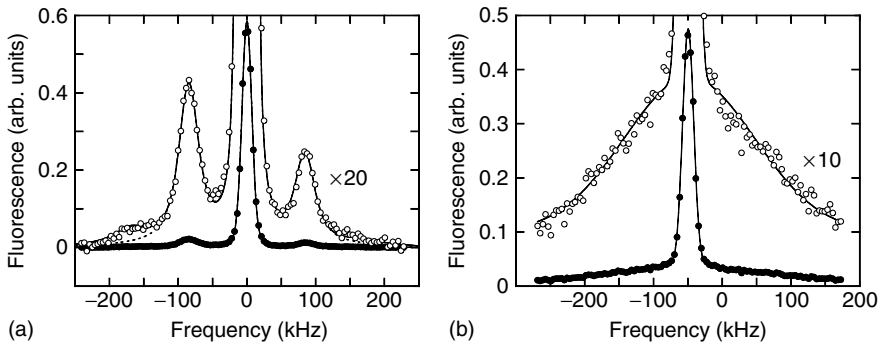

Fig. 15 (a) Fluorescence spectrum in a 1-D lin ⊥ lin optical molasses. Atoms are first captured and cooled in an MOT, and then the MOT light beams are switched off leaving a pair of lin ⊥ lin because of spontaneous emission of the atoms to the same vibrational state from which they are excited, whereas the sideband on the left (right) is due to spontaneous emission to a vibrational state with one vibrational quantum number lower (higher) (see Fig. 13). The presence of these sidebands is a direct proof of the existence of the band structure. (b) Same as (a) except that the 1-D molasses is $\sigma^+ - \sigma^-$, which has no spatially dependent light shift and hence no vibrational states (figure taken from Jessen, P. S., Gerz, C., Lett, P. D., Phillips, W. D., Rolston, S. L., Spreeuw, R. J. C., Westbrook, C. I. (**1992**), *Phys. Rev. Lett.* **69**, 49–52)

$2n$. The real benefit of this scheme is that in case of phase instabilities in the laser beams, the interference pattern is only shifted in space, but the interference pattern itself is not changed. Instead of producing optical wells in 2-D with four beams (two standing waves), these authors used only three. The $\vec{k}$-vectors of the coplanar beams were separated by $2\pi/3$, and they were all linearly polarized in their common plane (not parallel to one another). The same immunity to vibrations was established for a 3-D optical lattice by using only four beams arranged in a quasi-tetrahedral configuration. The three linearly polarized beams of the 2-D arrangement described above were directed out of the plane toward a common vertex, and a fourth circularly polarized beam was added. All four beams were polarized in the same plane [68]. The authors showed that this configuration produced the desired potential wells in 3-D.

5.3 Spectroscopy in 3-D Lattices

The group at NIST developed a new method that superposed a weak probe beam of light directly from the laser upon some of the fluorescent light from the atoms in a 3-D OM, and directed the light from these combined sources onto on a fast photodetector [70]. The resulting beat signal carried information about the Doppler shifts of the atoms in the optical lattices [61]. These Doppler shifts were expected to be in the sub-MHz range for atoms with the previously measured 50-μK temperatures. The observed features confirmed the quantum nature of the motion of atoms in the wavelength-size potential wells (see Fig. 15) [15].

The NIST group also studied atoms loaded into an optical lattice using Bragg diffraction of laser light from the spatially ordered array [71]. They cut off the laser beams that formed the lattice, and before

the atoms had time to move away from their positions, they pulsed on a probe laser beam at the Bragg angle appropriate for one of the sets of lattice planes. The Bragg diffraction not only enhanced the reflection of the probe beam by a factor of 10^5, but by varying the time between the shut-off of the lattice and turn-on of the probe, they could also measure the ''temperature'' of the atoms in the lattice. The reduction of the amplitude of the Bragg-scattered beam with time provided some measure of the diffusion of the atoms away from the lattice sites, much like the Debye–Waller factor in X-ray diffraction.

5.4 Quantum Transport in Optical Lattices

In the 1930s, Bloch realized that applying a uniform force to a particle in a periodic potential would not accelerate it beyond a certain speed, but instead would result in Bragg reflection when its deBroglie wavelength became equal to the lattice period. Thus, an electric field applied to a conductor could not accelerate electrons to a speed faster than that corresponding to the edge of a Brillouin zone, and that at longer times the particles would execute oscillatory motion. Ever since then, experimentalists have tried to observe these Bloch oscillations in increasingly pure and/or defect-free crystals.

Atoms moving in optical lattices are ideally suited for such an experiment, as was beautifully demonstrated in 1996 [69]. The authors loaded a 1-D lattice with atoms from a 3-D molasses, further narrowed the velocity distribution, and then instead of applying a constant force, simply changed the frequency of one of the beams of the 1-D lattice with respect to the other in a controlled way, thereby creating an accelerating lattice. Seen from the atomic reference frame, this was the equivalent of a constant force trying to accelerate them. After a variable time t_a, the 1-D lattice beams were shut off and the measured atomic velocity distribution showed beautiful Bloch oscillations as a function of t_a. The centroid of the very narrow velocity distribution was seen to shift in velocity space at a constant rate until it reached

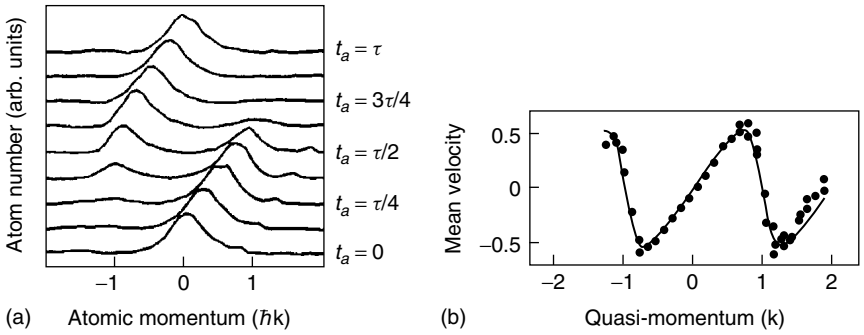

Fig. 16 Plot of the measured velocity distribution *verses*. time in the accelerated 1-D lattice. (a) Atoms in a 1-D lattice are accelerated for a fixed potential depth for a certain time t_a and the momentum of the atoms after the acceleration is measured. The atoms accelerate only to the edge of the Brillouin zone where the velocity is $+\nu_r$, and then the velocity distribution appears at $-\nu_r$. (b) Mean velocity of the atoms as a function of the quasi-momentum, that is, the force times the acceleration time (figure taken from Ben Dahan, M., Peik, E., Reichel, J., Castin, Y., Salomon, C. (**1996**), *Phys. Rev. Lett.* **76**, 4508–4511)

$v_r = \hbar k/M$, and then it vanished and reappeared at $-v_r$ as shown in Fig. 16. The shape of the "dispersion curve" allowed measurement of the "effective mass" of the atoms bound in the lattice.

6 Bose–Einstein Condensation

6.1 Introduction

In the 1920s, Bose and Einstein predicted that for sufficiently high phase space density, $\rho_\phi \sim 1$ (see Sect. 1.2), a gas of atoms undergoes a phase transition that is now called Bose–Einstein condensation. It took 70 years before BEC could be unambiguously observed in a dilute gas. From the advent of laser cooling and trapping, it became clear that this method could be instrumental in achieving BEC.

BEC is another manifestation of quantization of atomic motion. It occurs in the absence of resonant light, and its onset is characterized by cooling to the point where the atomic deBroglie wavelengths are comparable to the interatomic spacing. This is in contrast with the topics discussed in Sect. 5 where the atoms were in an optical field and their deBroglie wavelengths were comparable to the optical wavelength λ.

Laser cooling alone is inherently incapable of achieving $\rho_\phi \sim 1$. This is easily seen from the recoil limit of Sect. 3.3.4 that limits λ_{deB} to λ/"few". Since the cross section for optical absorption near resonance is $\sigma \sim \lambda^2$ near $\rho_\phi \sim 1$, this limit of $\lambda_{deB} \sim \lambda$/"few" results in the penetration depth of the cooling light into the sample being smaller than λ. Thus, the sample would have to be extremely small and contain only a few atoms, hardly a system suitable for investigation.

Temperatures lower than the recoil limit are readily achieved by evaporative cooling, and so all BEC experiments employ it in their final phase. Evaporative cooling is inherently different from the other cooling processes discussed in Sect. 3, and hence discussed here separately.

Since the first observations in 1995, BEC has been the subject of intense investigation, both theoretical and experimental. No attempt is made in this article to even address, much less cover, the very rich range of physical phenomena that have been unveiled by these studies. Instead, we focus on the methods to achieve $\rho_\phi \sim 1$ and BEC.

6.2 Evaporative Cooling

Evaporative cooling is based on the preferential removal of those atoms from a confined sample with an energy higher than the average energy followed by a rethermalization of the remaining gas by elastic collisions. Although evaporation is a process that occurs in nature, it was applied to atom cooling for the first time in 1988 [72].

One way to think about evaporative cooling is to consider cooling of a container of hot liquid. Since the most energetic molecules evaporate from the liquid and leave the container, the remaining molecules obtain a lower temperature and are cooled. Furthermore, it requires the evaporation of only a small fraction of the liquid to cool it by a considerable amount.

Evaporative cooling works by removing the higher-energy atoms as suggested schematically in Fig. 17. Those that remain have much lower average energy (temperature) and so they occupy a smaller volume near the bottom of the

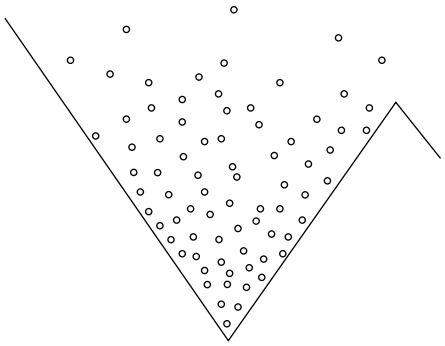

Fig. 17 Principle of the evaporation technique. Once the trap depth is lowered, atoms with energy above the trap depth can escape and the remaining atoms reach a lower temperature

trap, thereby increasing their density. For trapped atoms, it can be achieved by lowering the depth of the trap, thereby allowing the atoms with energies higher than the trap depth to escape, as discussed first by Hess [73]. Elastic collisions in the trap then lead to a rethermalization of the gas. This technique was first employed for evaporative cooling of hydrogen [72, 74–76]. Since both the temperature and the volume decrease, ρ_ϕ increases.

Recently, more refined techniques have been developed. For example, to sustain the cooling process the trap depth can be lowered continuously, achieving a continuous decrease in temperature. Such a process is called *forced evaporation* and is discussed in Sect. 6.3 below.

6.2.1 Simple Model

This section describes a simple model of evaporative cooling. Since such cooling is not achieved for single atoms but for the whole ensemble, an atomic description of the cooling process must be replaced by thermodynamic methods. These methods are completely different from the rest of the material in this article, and will therefore remain rather elementary.

Several models have been developed to describe this process, but we present here the simplest one [77] because of its pedagogical value [22]. In this model, the trap depth is lowered in one single step and the effect on the thermodynamic quantities, such as temperature, density, and volume, is calculated. The process can be repeated and the effects of multiple steps added up cumulatively.

In such models of evaporative cooling, the following assumptions are made:

1. The gas behaves sufficiently ergodically, that is, the distribution of atoms in phase space (both position and momentum) depends only on the energy of the atoms and the nature of the trap.
2. The gas is assumed to begin the process with $\rho_\phi \ll 1$ (far from the BEC transition point), and so it is described by classical statistics.
3. Even though $\rho_\phi \ll 1$, the gas is cold enough that the atomic scattering is pure (s-wave) quantum mechanical, that is, the temperature is sufficiently low that all higher partial waves do not contribute to the cross section. Furthermore, the cross section for elastic scattering is energy-independent and is given by $\sigma = 8\pi a^2$, where a is the scattering length. It is also assumed that the ratio of elastic to inelastic collision rates is sufficiently large that the elastic collisions dominate.
4. Evaporation preserves the thermal nature of the distribution, that is, the thermalization is much faster than the rate of cooling.
5. Atoms that escape from the trap neither collide with the remaining atoms nor exchange energy with them. This is called *full evaporation*.

6.2.2 Application of the Simple Model

The first step in applying this simple model is to characterize the trap by calculating how the volume of a trapped sample of atoms changes with temperature T. Consider a trapping potential that can be expressed as a power law given by

$$U(x,y,z) = \varepsilon_1 \left|\frac{x}{a_1}\right|^{s_1} + \varepsilon_2 \left|\frac{y}{a_2}\right|^{s_2} + \varepsilon_3 \left|\frac{z}{a_3}\right|^{s_3}, \quad (26)$$

where a_j is a characteristic length and s_j the power, for a certain direction j. Then the volume occupied by trapped atoms scales as $V \propto T^{\xi}$ [78], where

$$\xi \equiv \frac{1}{s_1} + \frac{1}{s_2} + \frac{1}{s_3}. \quad (27)$$

Thus, the effect of the potential on the volume of the trapped sample for a given temperature can be reduced to a single parameter ξ. This parameter is independent of how the occupied volume is defined, since many different definitions lead to the same scaling. When a gas is held in a 3-D box with infinitely high walls, then $s_1 = s_2 = s_3 = \infty$ and $\xi = 0$, which means that V is independent of T, as expected. For a harmonic potential in 3-D, $\xi = 3/2$; for a linear potential in 2-D, $\xi = 2$; and for a linear potential in 3-D, $\xi = 3$.

The evaporative cooling model itself [77] starts with a sample of N atoms in volume V having a temperature T held in an infinitely deep trap. The strategy for using the model is to choose a finite quantity η, and then (1) lower the trap depth to a value $\eta k_B T$, (2) allow for a thermalization of the sample by collisions, and (3) determine the change in ρ_ϕ.

Only two parameters are needed to completely determine all the thermodynamic quantities for this process (the values after the process are denoted by a prime). One of these is $\nu \equiv N'/N$, the fraction of atoms remaining in the trap after the cooling. The other is γ (This γ is not to be confused with the natural width of the excited state.), a measure of the decrease in temperature caused by the release of hot atoms and subsequent cooling, modified by ν, and defined as

$$\gamma \equiv \frac{\log(T'/T)}{\log(N'/N)} = \frac{\log(T'/T)}{\log \nu}. \quad (28)$$

This yields a power-law dependence for the decrease in temperature caused by the loss of the evaporated particles, that is, $T' = T\nu^{\gamma}$. The dependence of the other thermodynamic quantities on the parameters ν and γ can then be calculated.

The scaling of $N' = N\nu$, $T' = T\nu^{\gamma}$, and $V' = V\nu^{\gamma\xi}$ can provide the scaling of all the other thermodynamic quantities of interest by using the definitions for the density $n = N/V$, the phase space density $\rho_\phi = n\lambda_{\mathrm{deB}}^3 \propto nT^{-3/2}$, and the elastic collision rate $k_{\mathrm{el}} \equiv n\sigma v \propto nT^{1/2}$. The results are given in Table 2. For a given value of η, the scaling of all quantities

Tab. 2 Exponent q for the scaling of the thermodynamic quantities $X' = X\nu^q$ with the reduction ν of the number of atoms in the trap

Thermodynamic variable	*Symbol*	*Exponent q*
Number of atoms	N	1
Temperature	T	γ
Volume	V	$\gamma\xi$
Density	n	$1-\gamma\xi$
Phase space density	ρ	$1-\gamma(\xi+3/2)$
Collision rate	k	$1-\gamma(\xi-1/2)$

depends only on γ. Note that for successive steps j, ν has to be replaced with ν^j.

The fraction of atoms remaining is fully determined by the final trap depth η for a given potential characterized by the trap parameter ξ. In order to determine the change of the temperature in the cooling process, it is necessary to consider in detail the distribution of the atoms in the trap, and this is discussed more fully in Refs. [1, 22, 77].

6.2.3 Speed of Evaporation

So far, the speed of the evaporative cooling process has not been considered. If the trap depth is ramped down too quickly, the thermalization process does not have time to run its course and the process becomes less efficient. On the other hand, if the trap depth is ramped down too slowly, the loss of particles by inelastic collisions becomes important, thereby making the evaporation inefficient.

The speed of evaporation can be found from the principle of detailed balance[22]. Its application shows that the ratio of the evaporation time and the elastic collision time is

$$\frac{\tau_{\mathrm{ev}}}{\tau_{\mathrm{el}}} = \frac{\sqrt{2}e^{\eta}}{\eta}. \tag{29}$$

Note that this ratio increases exponentially with η.

Experimental results show that ~2.7 elastic collisions are necessary to rethermalize the gas [79]. In order to model the rethermalization process, Luiten et al [80] have discussed a model based on the Boltzmann equation where the evolution of the phase space density $\rho(\vec{r}, \vec{p}, t)$ is calculated. This evolution is not only caused by the trapping potential, but also by collisions between the particles. Only elastic collisions, whose cross section is given by $\sigma = 8\pi a^2$ with a as the scattering length, are considered. This leads to the Boltzmann equation [81].

6.2.4 Limiting Temperature

In the models discussed so far, only elastic collisions have been considered, that is, collisions where kinetic energy is redistributed between the partners. However, if part of the internal energy of the colliding partners is exchanged with their kinetic energy during •collision, then it is inelastic. Inelastic collisions can cause problems for two reasons: (1) the internal energy released can cause the atoms to heat up and (2) the atoms can change their internal states, and the new states may no longer be trapped. In each case, such collisions can lead to trap loss and are therefore not desirable. Q12

Apart from collisions with the background gas and three-body recombination, there are two inelastic processes that are important for evaporative cooling of alkali atoms: dipolar relaxation and spin relaxation. The collision rate nk_{dip} for them at low energies is independent of velocity [82]. Since the elastic collision rate is given by $k_{\mathrm{el}} = n\sigma v_{\mathrm{rel}}$, the ratio of good (= elastic) to bad (= relaxation) collisions goes down when the temperature does. This limits the temperature to a value T_e near which •the ratio between good and bad collisions becomes unity, and T_e is given by Q13

$$k_{\mathrm{B}} T_e = \frac{\pi M k_{\mathrm{dip}}^2}{16\sigma^2}. \tag{30}$$

The limiting temperature for the alkalis is of the order of 1 nK, depending on the values of σ and k_{dip}.

In practice, however, this ratio has to be considerably larger than unity, and so the practical limit for evaporative cooling occurs when the ratio is $\sim 10^3$ [22].

In the model of Ref. [80], the authors discuss different strategies for evaporative cooling. Even for the strategy of the lowest temperature, the final temperature is higher than T_e.

The collision rate between atoms with one in the excited state (S + P collisions) is also much larger at low temperatures than the rate for such collisions with both atoms in the ground state (S + S collisions). Since S + P collisions are generally inelastic and the inelastic energy exchange generally leads to a heating of the atoms, increasing the density increases the loss of cold atoms. To achieve BEC, resonant light should therefore be avoided, and thus laser cooling is not suitable for achieving BEC.

6.3 Forced Evaporative Cooling

In all the earliest experiments that achieved BEC, the evaporative cooling was "forced" by inducing rf transitions to magnetic sublevels that are not bound in the magnetic trap. Atoms with the highest energies can access regions of the trap where the magnetic field is stronger, and thus their Zeeman shifts would be larger. A correspondingly high-frequency rf field would cause only these most energetic atoms to undergo transitions to states that are not trapped, and in doing so, the departing atoms carry away more than the average energy. Thus, a slow sweep of the rf frequency from high to low would continuously shave off the high-energy tail of the energy distribution, and thereby continuously drive the temperature lower and the phase space density higher. The results of evaporative cooling from the first three groups that have obtained BEC have shown that using this rf shaving technique, it is much easier to select high-energy atoms and waste them than it is to cool them.

For the evaporation of the atoms, it is important that atoms with an energy above the cutoff are expelled from the trap. By using RF-evaporation, one can expel the atoms in all three dimensions equally and thus obtain a true 3-D evaporation. In the case of the TOP•-trap, the atoms are evaporated along the outer side of the cloud that is exposed to the highest magnetic field on the average. This is a cylinder along the direction of rotation axis of the magnetic field and thus the evaporation takes place in 2-D. Q14

Once the energy of the atoms becomes very small, the atoms sag because of gravity and the outer shell of the cloud is no longer at a constant magnetic field. Atoms at the bottom of the trap have the highest energy and thus the evaporation becomes 1-D. In case of harmonic confinement, $U_{\text{trap}} = U''z^2/2$, the equipotential surface is at $z \approx \sqrt{2\eta k_B T/U''}$. Now, the gravitational energy is given by $U_{grav} = mgz$ and thus the limiting temperature for 1-D evaporation to take place is given by [22]

$$k_B T < \frac{2\eta(mg)^2}{\mu B''} \tag{31}$$

For a curvature of $B'' = 500\ \text{T m}^{-2}$, the limiting temperature becomes 1 μK for ^{7}Li, 10 μK for ^{23}Na, and 150 μK for ^{87}Rb. Below this temperature, evaporation becomes less efficient.

In the three experiments that obtained BEC for the first time in 1995, the problem of this "gravitational sag" was not known, but it did not prevent the experimentalist from observing BEC. The solution used in those experiments was because of the light mass (^{7}Li), tight confinement (^{23}Na), and TOP trap (^{87}Rb). In the last case, the axis of rotation is in the z-direction and

Tab. 3 Typical numbers for the phase space density as obtained in the experiments aimed at achieving BEC. The different stages of cooling and trapping the atoms will be discussed in the Appendix

Stages	*T*	λ_{deB}	*n*	ρ_ϕ
Oven	300 °C	0.02 nm	10^{10} cm^{-3}	10^{-16}
Slowing	30 mK	2 nm	10^{8} cm^{-3}	10^{-12}
Pre-cooling	1 mK	10 nm	10^{9} cm^{-3}	10^{-9}
Trapping	1 mK	10 nm	10^{12} cm^{-3}	10^{-6}
Cooling	1 µK	0.3 µm	10^{11} cm^{-3}	3×10^{-3}
Evaporation	70 nK	1 µm	10^{12} cm^{-3}	2.612

thus the evaporation always remains 2-D. Table 3 shows typical values of ρ_ϕ for various situations.

7 Conclusion

In this article, we have reviewed some of the fundamentals of optical control of atomic motion. The reader is cautioned that this is by no means an exhaustive review of the field, and that many important and current topics have been omitted. Much of the material here was taken from our recent textbook [1], and the reader is encouraged to consult that source for the origin of many of the formulas presented in the present text, as well as for further reading and more detailed references to the literature.

References

[1] Metcalf, H. J., vander Straten, P. (1999), *Laser Cooling and Trapping*. New York: Springer-Verlag.
[2] Phillips, W., Metcalf, H. (**1982**), *Phys. Rev. Lett.* **48**, 596–599.
[3] Prodan, J., Phillips, W., Metcalf, H. (**1982**), *Phys. Rev. Lett.* **49**, 1149–1153.
[4] Prodan, J., Phillips, W. (**1984**), *Prog. Quant. Electron.* **8**, 231–235.
[5] Ertmer, W., Blatt, R., Hall, J. L., Zhu, M. (**1985**), *Phys. Rev. Lett.* **54**, 996–999.
[6] Watts, R., Wieman, C. (**1986**), *Opt. Lett.* **11**, 291–293.
[7] Bagnato, V., Lafyatis, G., Martin, A., Raab, E., Ahmad-Bitar, R., Pritchard, D. (**1987**), *Phys. Rev. Lett.* **58**, 2194–2197.
[8] Molenaar, P. A., vander Straten, P., Heideman, H. G. M., Metcalf, H. (**1997**), *Phys. Rev. A* **55**, 605–614.
[9] Barrett, T. E., Dapore-Schwartz, S. W., Ray, M. D., Lafyatis, G. P. (**1991**), *Phys. Rev. Lett.* **67**, 3483–3487.
[10] Dalibard, J., Phillips, W. (**1985**), *Bull. Am. Phys. Soc.* **30**, 748.
[11] Chu, S., Hollberg, L., Bjorkholm, J., Cable, A., Ashkin, A. (**1985**), *Phys. Rev. Lett.* **55**, 48–51.
[12] Sheehy, B., Shang, S. Q., vander Straten, P. Metcalf, H. (**1990**), *Chem. Phys.* **145**, 317–325.
[13] Gould, P., Lett, P., Phillips, W. D. (1987), New measurement with optical molasses, in W. Persson, S. Svanberg, (Eds.), *Laser Spectroscopy VIII*, Berlin: Springer, p. 64●.
[14] Hodapp, T., Gerz, C., Westbrook, C., Furlehner, C., Phillips, W. (**1992**), *Bull. Am. Phys. Soc.* **37**, 1139.
[15] Lett, P., Watts, R., Westbrook, C., Phillips, W., Gould, P., Metcalf, H. (**1988**), *Phys. Rev. Lett.* **61**, 169–172.
[16] Lett, P. D., Watts, R. N., Tanner, C. E., Rolston, S. L., Phillips, W. D., Westbrook, C. I. (**1989**), *J. Opt. Soc. Am. B* **6**, 2084–2107.
[17] Dalibard, J., Cohen-Tannoudji, C. (**1989**), *J. Opt. Soc. Am. B* **6**, 2023–2045.
[18] Ungar, P. J., Weiss, D. S., Chu, S., Riis, E. (**1989**), *J. Opt. Soc. Am. B* **6**, 2058–2071.

Q15

[19] Cohen-Tannoudji, C., Phillips, W. D. (**1990**), *Phys. Today* **43**, 33–40.
[20] Gupta, R., Padua, S., Xie, C., Batelaan, H., Metcalf, H. (**1994**), *J. Opt. Soc. Am. B* **11**, 537–541.
[21] Salomon, C., Dalibard, J., Phillips, W. D., Clairon, A., Guellati, S. (**1990**), *Europhys. Lett.* **12**, 683–688.
[22] Ketterle, W., Vandruten, N. J. (**1996**), *Adv. At. Mol. Opt. Phys.* **37**, 181–236.
[23] Aspect, A., Arimondo, E., Kaiser, R., Vansteenkiste, N., Cohen-Tannoudji, C. (**1988**), *Phys. Rev. Lett.* **61**, 826–829.
[24] Kasevich, M., Chu, S. (**1992**), *Phys. Rev. Lett.* **69**, 1741–1744.
[25] Ashkin, A. (**1970**), *Phys. Rev. Lett.* **24**, 156–159.
[26] Chu, S., Bjorkholm, J., Ashkin, A., Cable, A. (**1986**), *Phys. Rev. Lett.* **57**, 314–317.
[27] Ashkin, A. (**1980**), *Science* **210**, 1081–1088.
[28] Ashkin, A., Dziedzic, J. M. (**1985**), *Phys. Rev. Lett.* **54**, 1245–1248.
[29] Ashkin, A., Dziedzic, J. M. (**1987**), *Science* **235**, 1517–1520.
[30] Miller, J. D., Cline, R. A., Heinzen, D. J. (**1993**), *Phys. Rev. A* **47**, R4567–R4570.
[31] Adams, C. S., Lee, H. J., Davidson, N., Kasevich, M., Chu, S. (**1995**), *Phys. Rev. Lett.* **74**, 3577–3580.
[32] Takekoshi, T., Knize, R. J. (**1996**), *Opt. Lett.* **21**, 77–79.
[33] Metcalf, H., Phillips, W. (**1986**), *Metrologia* **22**, 271–278.
[34] Davidson, N., Lee, H. J., Adams, C. S., Kasevich, M., Chu, S. (**1995**), *Phys. Rev. Lett.* **74**, 1311–1314.
[35] Siegman, A. (1986), *Lasers.* Mill Valley: University Sciences.
[36] Simpson, N., Dholakia, K., Allen, L., Padgett, M. (**1997**), *Opt. Lett.* **22**, 52–54.
[37] McGloin, D., Simpson, N., Padgett, M. (**1998**), *App. Opt.* **37**, 469–472.
[38] Beijersbergen, M. (1996), Phase Singularities in Optical Beams. Ph.D. Thesis, University Leiden●.
[39] Ovchinnikov, Yu. B., Manek, I. Grimm, R. (**1997**), *Phys. Rev. Lett.* **79**, 2225–2228.
[40] Aminoff, C. G., Steane, A. M., Bouyer, P., Desbiolles, P., Dalibard, J., Cohen-Tannoudji, C. (**1993**), *Phys. Rev. Lett.* **71**, 3083–3086.
[41] Kasevich, M. A., Weiss, D. S., Chu, S. (**1990**), *Opt. Lett.* **15**, 607–609.
[42] Wineland, D., Itano, W., Bergquist, J., Bollinger, J. (1985), Trapped Ions and Laser Cooling. Technical Report 1086, N.I.S.T.●.
[43] Migdall, A., Prodan, J., Phillips, W., Bergeman, T., Metcalf, H. (**1985**), *Phys. Rev. Lett.* **54**, 2596.
[44] Bergeman, T., Erez, G., Metcalf, H. (**1987**), *Phys. Rev. A* **35**, 1535.
[45] Bergeman, T. H., Balazs, N. L., Metcalf, H., Mcnicholl, P., Kycia, J. (**1989**), *J. Opt. Soc. Am. B* **6**, 2249–2256.
[46] Raab, E., Prentiss, M., Cable, A., Chu, S., Pritchard, D. (**1987**), *Phys. Rev. Lett.* **59**, 2631–2634.
[47] Metcalf, H. (**1989**), *J. Opt. Soc. Am. B* **6**, 2206–2210.
[48] Molenaar, P. (1995), Photoassociative Reactions of Laser-Cooled Sodium. Ph.D. Thesis, Utrecht University●.
[49] Cornell, E. A., Monroe, C., Wieman, C. E. (**1991**), *Phys. Rev. Lett.* **67**, 2439–2442.
[50] Steane, A. M., Foot, C. J. (**1991**), *Europhys. Lett.* **14**, 231–236.
[51] Steane, A. M., Chowdhury, M., Foot, C. J. (**1992**), *J. Opt. Soc. Am. B* **9**, 2142–2158.
[52] Gould, P. private communication●.
[53] Walker, T., Sesko, D., Wieman, C. (**1990**), *Phys. Rev. Lett.* **64**, 408–411.
[54] Sesko, D. W., Walker, T. G., Wieman, C. E. (**1991**), *J. Opt. Soc. Am. B* **8**, 946–958.
[55] Gibble, K. E., Kasapi, S., Chu, S. (**1992**), *Opt. Lett.* **17**, 526–528.
[56] Lindquist, K., Stephens, M., Wieman, C. (**1992**), *Phys. Rev. A* **46**, 4082–4090.
[57] Ketterle, W., Davis, K. B., Joffe, M. A., Martin, A., Pritchard, D. E. (**1993**), *Phys. Rev. Lett.* **70**, 2253–2256.
[58] Lethokov, V. S. (**1968**), *JETP Lett.* **7**, 272.
[59] Salomon, C., Dalibard, J., Aspect, A., Metcalf, H., Cohen-Tannoudji, C. (**1987**), *Phys. Rev. Lett.* **59**, 1659–1662.
[60] Castin, Y., Dalibard, J. (**1991**), *Europhys. Lett.* **14**, 761–766.
[61] Jessen, P. S., Gerz, C., Lett, P. D., Phillips, W. D., Rolston, S. L., Spreeuw, R. J. C., Westbrook, C. I. (**1992**), *Phys. Rev. Lett.* **69**, 49–52.
[62] Verkerk, P., Lounis, B., Salomon, C., Cohen-Tannoudji, C., Courtois, J. Y., Grynberg, G. (**1992**), *Phys. Rev. Lett.* **68**, 3861–3864.
[63] Lounis, B., Verkerk, P., Courtois, J. Y., Salomon, C., Grynberg, G. (**1993**), 1-D *Europhys. Lett.* **21**, 13–17.

Q16 Q17 Q18 Q19

[64] Gupta, R., Padua, S., Xie, C., Batelaan, H., Bergeman, T., Metcalf, H. (**1992**), *Bull. Am. Phys. Soc.* **37**, 1139.
[65] Gupta, R., Padua, S., Bergeman, T., Metcalf, H. (1993), Search for motional quantization of laser-cooled atoms, in E. Arimondo, W. Phillips, F. Strumia (Eds.), *Laser Manipulation of Atoms and Ions, Proceedings of Fermi School CXVIII, Varenna,* Amsterdam: North Holland.
[66] Anderson, B. P., Kasevich, M. A. (**1998**), *Nature* **282**, 1686–1689.
[67] Greiner, M., Mandel, O., Esslinger, T., Hänsch, T. W., Bloch, I. (**2002**), *Nature* **415**, 39–44.
[68] Grynberg, G., Lounis, B., Verkerk, P., Courtois, J. Y., Salomon, C. (**1993**), *Phys. Rev. Lett.* **70**, 2249–2252.
[69] Ben Dahan, M., Peik, E., Reichel, J., Castin, Y., Salomon C. (**1996**), *Phys. Rev. Lett.* **76**, 4508–4511.
[70] Westbrook, C. I., Watts, R. N., Tanner, C. E., Rolston, S. L., Phillips, W. D., Lett, P. D., Gould, P. L. (**1990**), *Phys. Rev. Lett.* **65**, 33–36.
[71] Birkl, G., Gatzke, M., Deutsch, I. H., Rolston, S. L., Phillips, W. D. (**1995**), *Phys. Rev. Lett.* **75**, 2823–2826.
[72] Masuhara, N., Doyle, J. M., Sandberg, J. C., Kleppner, D., Greytak, T. J., Hess, H. F., Kochanski, G. P. (**1988**), *Phys. Rev. Lett.* **61**, 935.
[73] Hess, H. F. (**1986**), *Phys. Rev. B* **34**, 3476.
[74] Doyle, J. M., Sandberg, J. C., Yu, I. A., Cesar, C. L., Kleppner, D., Greytak, T. J. (**1991**), *Phys. Rev. Lett.* **67**, 603.
[75] Luiten, O. J., Werij, H. G. C., Setija, I. D., Reynolds, M. W., Hijmans, T. W., Walraven, J. T. M. (**1993**), *Phys. Rev. Lett.* **70**, 544–547.
[76] Setija, I. D., Werij, H. G. C., Luiten, O. J., Reynolds, M. W., Hijmans, T. W., Walraven, J. T. M. (**1993**), *Phys. Rev. Lett.* **70**, 2257–2260.
[77] Davis, K. B., Mewes, M. O., Ketterle, W. (**1995**), *App. Phys. B* **60**, 155–159.
[78] Bagnato, V., Pritchard, D. E., Kleppner, D. (**1987**), *Phys. Rev. A* **35**, 4354.
[79] Monroe, C., Cornell, E., Sackett, C., Myatt, C., Wieman, C. (**1993**), *Phys. Rev. Lett.* **70**, 414.
[80] Luiten, O. J., Reynolds, M. W., Walraven, J. T. M. (**1996**), *Phys. Rev. A* **53**, 381.
[81] Huang, K. (1963), *Statistical Mechanics.* New York: Wiley.
[82] Landau, L. D., Lifshitz, E. M. (1958), *Quantum Mechanics (Non-Relativistic Theory)*. Oxford: Pergamon Press.